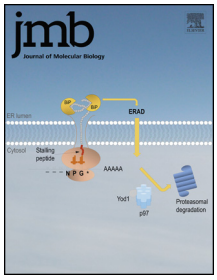

The Fibrillin-1 RGD Integrin Binding Site Regulates Gene Expression and Cell Function through microRNAs

Karina A. Zeyer[1,†], **Rong-Mo Zhang**[1,†], **Heena Kumra**[1], **Amani Hassan**[1] and **Dieter P. Reinhardt**[1,2]

*1 - **Faculty of Medicine,** McGill University, Montreal, Canada*
*2 - **Faculty of Dentistry,** McGill University, Montreal, Canada*

***Correspondence to Dieter P. Reinhardt:** Department of Anatomy and Cell Biology, McGill University, 3640 University Street, Montreal, Quebec H3A 0C7, Canada. dieter.reinhardt@mcgill.ca*
https://doi.org/10.1016/j.jmb.2018.11.021
Edited by M Yaniv

Abstract

Fibrillins are the major components of microfibrils in the extracellular matrix of elastic and non-elastic tissues. Fibrillin-1 contains one evolutionarily conserved RGD sequence that mediates cell–matrix interactions through cell-surface integrins. Here, we present a novel paradigm how extracellular fibrillin-1 controls cellular function through integrin-mediated microRNA regulation. Comparative mRNA studies by global microarray analysis identified growth factor activity, actin binding and integrin binding as the most important functional groups that are regulated upon fibrillin-1 binding to dermal fibroblasts. Many of these mRNAs are targets of miRNAs that were identified when RNA from the fibrillin-1-ligated fibroblasts was analyzed by a miRNA microarray. The expression profile was specific to fibrillin-1 since interaction with fibronectin displayed a partially distinct profile. The importance of selected miRNAs for the regulation of the identified mRNAs was suggested by bioinformatics prediction and the interactions between miRNAs and mRNAs were experimentally validated. Functionally, we show that miR-503 controls p-Smad2-dependent TGF-β signaling, and that miR-612 and miR-3185 are involved in the focal adhesion formation regulated by fibrillin-1. In conclusion, we demonstrate that fibrillin-1 interaction with fibroblasts regulates miRNA expression profiles which in turn control critical cell functions.

Introduction

The fibrillin family consists of three highly homologous, evolutionarily conserved ~350 kDa glycoproteins, fibrillin-1, fibrillin-2 and fibrillin-3 [1–4]. Fibrillin-1 is the main form in postnatal life, whereas fibrillin-2 and fibrillin-3 are primarily expressed during development [5–7]. Fibrillins are multidomain proteins composed of common and unique domains, depicted in Supplemental Fig. S1A [8,9]. The most frequently occurring domains are calcium-binding epidermal growth factor-like (cbEGF) domains [10] and transforming growth factor-beta binding protein-like (TB) domains [11].

The fourth TB domain contains the sole RGD cell binding site in fibrillin-1. RGD sequences represent integrin receptor recognition sites that tether extracellular proteins to cells and mediate numerous cellular functions including cell attachment, focal adhesion formation and intracellular signaling [12,13]. This interaction is essential for cells to sense and react to their extracellular microenvironment [14,15]. Specifically, fibrillin-1 interacts with integrins $\alpha_5\beta_1$, $\alpha_v\beta_3$ and $\alpha_v\beta_6$ [16–19]. Fibrillin-1 adhesion to integrin $\alpha_5\beta_1$ and cell migration is enhanced by an upstream synergy site, comprised by a cbEGF array [20]. In addition, fibrillin-1 is a major heparin/heparan sulfate interacting protein, containing seven binding regions [21–25]. One heparan sulfate binding site, located immediately downstream of TB4, supports focal adhesion formation [20]. Supplemental Fig. S1A shows the RGD cell binding site, the synergy region and the heparan sulfate binding regions relative to the full-length fibrillin-1 protein.

Secreted fibrillins first associate with the cell surface [26], and then multimerize into supramolecular microfibrils in the extracellular matrix of elastic and non-elastic tissues. During development, microfibrils act

as a scaffold for tropoelastin deposition in skin, blood vessels and lung [27]. Microfibrils also occur independently of elastic fibers, for example, in ciliary zonules of the ocular system, or along basement zones in various tissues [28,29]. Importantly, microfibrils play a major fibrillin-1-associated role in regulating the bioavailability of growth factors of the transforming growth factor-beta (TGF-β) superfamily [30,31]. Whereas TGF-βs interact with fibrillin-1 and microfibrils indirectly in the extracellular matrix through interactions with the latent TGF-β binding protein (LTBP)-1, LTBP-3 and LTBP-4 [32], bone morphogenetic protein (BMP)-2, BMP-4, BMP-7 and BMP-10 interact directly with fibrillin-1 [31].

The importance of microfibrils in the development and homeostasis of tissues is highlighted by a variety of autosomal dominant connective tissue disorders caused by mutations in fibrillin-1, most importantly Marfan syndrome [33], but also other disorders such as stiff skin syndrome [34], acromicric and geleophysic dysplasia [35], and dominant Weill–Marchesani syndrome [36]. Deregulation of TGF-β is an important contributor to the pathogenesis in Marfan syndrome and related disorders [30,37].

Micro-ribonucleic acids (miRNAs) have been identified as important regulators of gene expression [38]. They represent single-stranded short non-coding RNAs that are about 21–23 nucleotides in length. Most miRNAs regulate gene expression on the mRNA level by binding directly to the 3′ untranslated regions (UTRs) of specific target mRNAs. This leads to the inhibition of translation through either mRNA cleavage or translational repression, or decreased mRNA stability as a result of deadenylation [39]. Inhibition of miRNAs maturation by ablating the RNaseIII catalytic domain of Dicer leads to stem cell depletion and embryonic lethality [40]. miRNAs are essential for the regulation of cellular activity. As key regulators of gene expression of many cellular processes, miRNAs can regulate 30%–60% of human genes [41]. miRNAs have been demonstrated to be involved in the regulation of extracellular matrix proteins and their receptors including collagens, fibronectin and integrins [42]; growth factor bioavailability [43]; and cytoskeletal dynamics [44]. Directly related to fibrillin-1, it was shown that miR-29b regulates aortic wall apoptosis and extracellular matrix abnormalities in the *Fbn1*$^{C1039G/+}$ Marfan syndrome mouse model [45]. An initial biological proof of concept study demonstrated that silencing miR-29b in these mice can prevent early aneurysm formation [46].

The relationship between miRNAs and the interaction of fibrillin-1 with integrins is currently not understood. This study identifies several miRNAs and delineates their role in cell functions triggered by cell–fibrillin-1 interactions. Unraveling the downstream pathways that are regulated by fibrillin-1 allows to understand the physiological function of fibrillin-1-mediated cell–matrix interactions at an early stage of microfibril assembly and pathology.

Results

RGD-mediated fibrillin-1 interaction with cells alters mRNA expression of growth factors, actin-binding proteins and integrins

Directly after secretion, fibrillin-1 associates with the cell surface where it co-localizes with fibronectin [26], prior to forming higher-molecular-weight assemblies [47]. We intended to mimic this early stage of monomeric fibrillin-1 cell association to analyze the cellular consequences on mRNA expression by microarray analysis (Affymetrix Human Gene 2.0 chips). For this reason, we produced two recombinant human fibrillin-1 fragments encompassing domains cbEGF10 to cbEGF31 (Supplemental Fig. S1A). The wild-type rF1M-WT fragment was designed to include the RGD integrin binding site in the TB4 domain, as well as the upstream located synergy region and two heparin-binding regions, to analyze the RGD cell binding site in its sequence context needed to properly mediate cell attachment and cell binding to fibrillin-1 [20]. Since the essential multimerization region in the fibrillin-1 C-terminus is absent in rF1M, it is not able form multimers [47]. The rF1M-RGA mutant fragment is identical to rF1M-WT except one point mutation (p.Asp1587Ala), which has been previously shown to abolish interaction with integrins [19,20]. This fragment was used as a non-cell interacting control. The microarray was conducted with RNA preparations obtained from human skin fibroblasts (HSFs) grown for 24 h on rF1M-WT and the rF1M-RGA control. To minimize potential interference of endogenously produced fibrillin-1 as well as fibronectin, which also contains an RGD sequence, we carefully analyzed primary fibroblasts from several donors for the levels of endogenously produced fibrillin-1 and fibronectin. For this study, we have selected fibroblasts displaying very little or no fibrillin-1 and fibronectin after 24 h (Supplemental Fig. S2). In addition, we have determined the optimal coating concentration for the recombinant fragments at 25 μg/mL (Supplemental Fig. S3), a concentration that is sufficiently high to outcompete remaining traces of endogenous fibrillin-1 and fibronectin.

Upon adhesion of HSFs to fibrillin-1, 520 differentially regulated mRNAs with a false determination rate (FDR)-adjusted p value of <0.05 were detected that were at least 2-fold significantly upregulated or downregulated (Fig. 1a). This demonstrates that fibrillin-1 binding via the RGD site triggers a broad cellular response. To predict enriched functional themes, gene ontology analysis of the selected gene products was employed using the database for

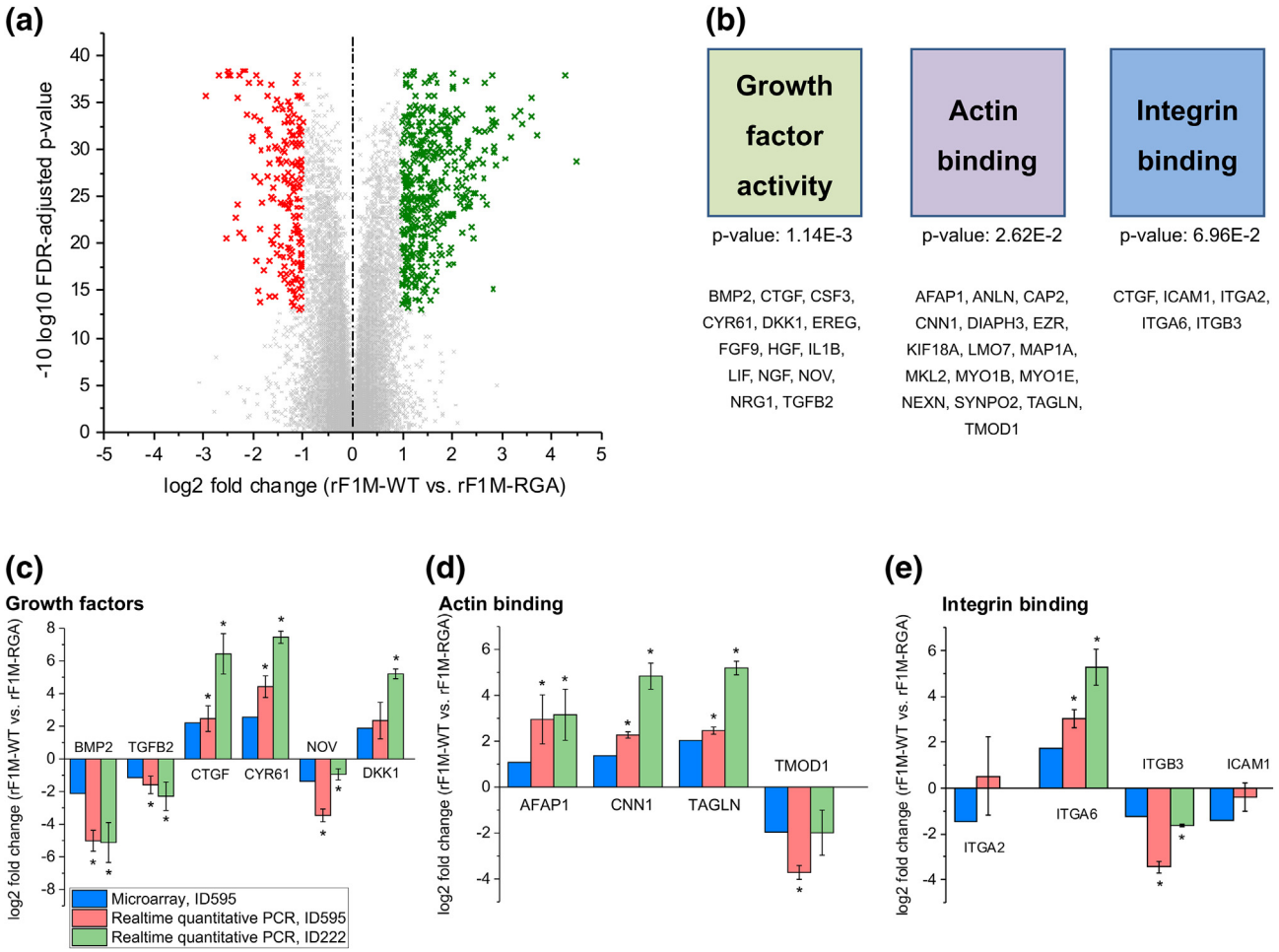

Fig. 1. Comparative analysis of fibroblast mRNA expression levels. (a) Microarray analysis was conducted for mRNAs in biological quadruplicates for each condition (rF1M-WT *versus* rF1M-RGA) using the Gene Chips Human Gene 2.0 (Affymetrix). Differential mRNA expression between the two conditions after 24 h is shown as a volcano plot. Statistically significant upregulated mRNAs are shown in green and downregulated mRNAs in red. Only mRNAs with a fold change of <-2 or >2 are considered. 520 differentially regulated mRNAs were detected. (b) Functional annotation was conducted to identify enriched biological themes for the 520 differentially expressed mRNAs using DAVID Bioinformatics Resources 6.7 (david.abcc.ncifcrf.gov) [80]. A selection of Gene Ontology (GO) terms of molecular function is shown including the respective *p* values. Dysregulated mRNAs within the respective GO groups are listed below. (c-e) Microarray validation by qPCR was conducted for selected mRNAs in each of the functional groups indicated in panel b. The functional groups include growth factors (c), actin binding (d) and integrin binding (e). HSFs from two different human donors were used to validate the results of the microarray (ID 595, ID 222). ID 595 was used in the microarray. The mRNA levels are shown as log2 fold changes of rF1M-WT *versus* rF1M-RGA. Values are indicated as mean values of biological triplicates with three technical replicates each ± SEM. Student's *t* test was performed to assess statistical significance (* $p < 0.05$).

annotation, visualization and integrated discovery (DAVID) Bioinformatics Resources, which identified growth factor activity, actin binding and integrin binding as relevant enriched groups, among others (Fig. 1b). These three groups were of particular interest for the following reasons. Growth factor regulation by the extracellular matrix is well established for growth factors of the TGF-β superfamily that are known to be sequestered by microfibrils. Two members of this group, *TGFB2* and *BMP2* mRNA, were identified in the microarray. Moreover, other growth factor mRNAs such as three members of the CCN gene family (*CTGF*, *CYR61*, *NOV* mRNAs) were found to be differentially regulated in the microarray analysis. Actin binding and integrin binding represent two important groups as the interaction of the RGD site with integrins results in changes in cell shape and adhesion compared to the RGA control (Supplemental Fig. S4A, C). Actin-binding proteins are likely relevant for these different phenotypes.

The Kyoto encyclopedia of genes and genomes (KEGG) pathway bioinformatic analysis narrows down the general description of the molecular function to a list of defined pathways. Table 1 displays a list of differentially regulated pathways relevant to fibrillin-1 binding and signaling. These include growth factor pathways such as TGF-β, mitogen-activated protein kinases (MAPK), Wnt, Hedgehog and Notch signaling, focal adhesions, and the regulation of the actin cytoskeleton.

mRNAs from these selected functional groups with relevance to fibrillin biology and/or with the highest fold changes upon fibrillin binding were validated by real-time qPCR using HSFs from two different human donors (Fig. 1c–e). One cell ID was identical to the one used for the microarray analysis (ID 595), and another one (ID 222) was used to determine the conservation of the observed mRNA regulation among HSFs from different donors. Within the three groups, 10 out of 14 mRNAs (*BMP2*, *TGFB2*, *CTGF*, *CYR61*, *NOV*, *AFAP1*, *CNN1*, *TAGLN*, *ITGA6* and *ITGB3*) could be validated in HSFs from both donors.

Analysis of miRNA expression patterns after RGD binding

The differentially regulated mRNAs upon fibrillin-1 interaction raised the question how these changes are regulated. One potent mechanism in gene regulation are miRNAs. The same 24 h RNA preparations were thus used for a miRNA microarray (Affymetrix miRNA 3.0) to identify miRNAs involved in regulating the differentially expressed mRNAs for growth factors, actin-binding proteins and integrins. We identified 129 differentially expressed miRNAs with an FDR-adjusted p value of <0.05 (Fig. 2a).

To determine common pathways regulated by these 129 miRNAs, pathway prediction analysis was conducted using the DNA intelligent analysis (DIANA) miRPath v.2.0 tool [48] (Table 1). The list of pathways was almost identical to the ones identified in the mRNA pathway analysis. This indicates that the differentially regulated miRNAs and mRNAs act together in the same pathways including the TGF-β, MAPK, Wnt, and Hedgehog signaling pathways, as well as focal adhesions and the regulation of the actin cytoskeleton.

Ten miRNAs were chosen for further analysis based on their level of differential expression, their high statistical significance and their importance in regulating the relevant functional groups identified in the mRNA microarray. These miRNAs were validated by qPCR. For the upregulated miRNAs, the results from the microarray were confirmed for four of five miRNAs (Fig. 2b). Similarly, four of five downregulated miRNAs could be validated (Fig. 2c). Time course analyses of the validated miRNAs were performed to determine at what time point the expression levels were consistently upregulated or downregulated between 2 and 24 h after exposure to fibrillin-1 (Fig. 2d). Most tested miRNAs (miR-4521, miR-612, miR-1208, miR-1231, miR-3185) consistently changed expression levels a short time (2–8 h) after HSF binding to rF1M-WT. Three of the miRNAs (miR-29b-1*, miR-424*, miR-503) required longer (24 h) for a consistent upregulation. This data helps

Table 1. KEGG pathway analysis for the mRNA and miRNA microarray

KEGG pathway	p Value mRNA microarray	No. of genes	p Value miRNA microarray	No. of miRNAs	No. of genes
TGF-β signaling pathway	1.14E−3	6	5.22E−4	29	36
MAPK signaling pathway	4.30E−2	8	2.52E−19	50	120
Wnt signaling pathway	1.01E−2	3	1.04E−10	39	73
Hedgehog signaling pathway	1.75E−2	2	2.96E−10	31	27
Notch signaling pathway	4.33E−2	2	Not significant	–	–
Focal adhesion	2.62E−2	6	1.42E−37	47	105
Regulation of actin cytoskeleton	1.87E−3	10	8.18E−12	46	96

Analysis of KEGG pathways using the data from the mRNA microarray (fold-change >2-fold) was performed with the DAVID Bioinformatics Resources 6.7 [80,84] and using the data from the miRNA microarray with the DIANA miRPath v.2.0 [48]. A selection of relevant KEGG pathways is shown.

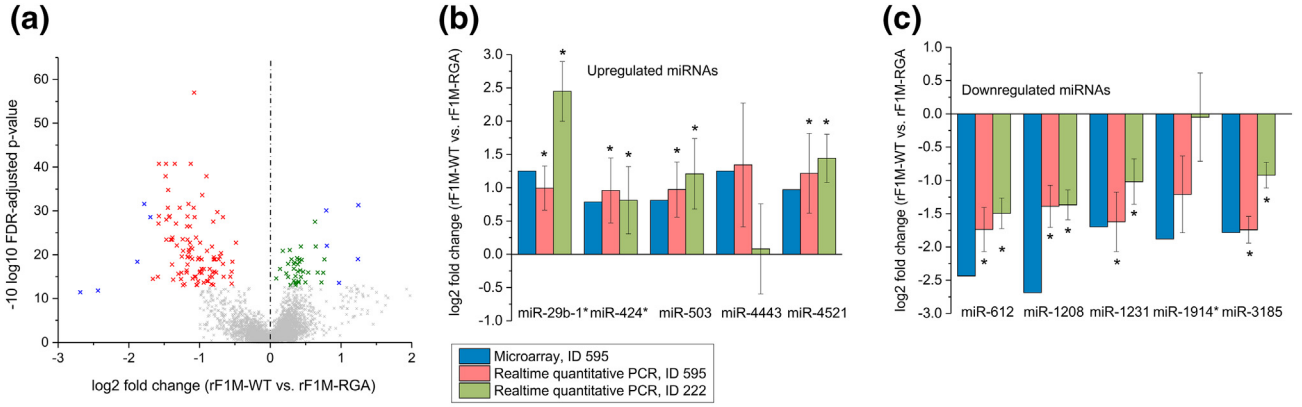

(d)

miRNAs	miR-29b-1*	miR-424*	miR-503	miR-4521	miR-612	miR-1208	miR-1231	miR-3185
Time	24 h	24 h	24 h	8 h	2 h	2 h	8 h	8 h

up-regulated miRNAs upon rF1M-WT binding

down-regulated miRNAs upon rF1M-WT binding

Fig. 2. Comparative analysis of fibroblast miRNA expression levels. (a) Microarray analysis of HSFs (ID 595) was conducted for miRNAs in biological quadruplicates for each condition using miRNA 3.0 chips (Affymetrix). RNA samples from the same HSFs (ID 595) exposed to the recombinant fibrillin-1 fragments for 24 h used for the mRNA microarray analysis (see Fig. 1a) were analyzed. Differential expression of miRNAs between the two conditions (rF1M-WT *versus* rF1M-RGA) after 24 h of cell growth is shown as a volcano plot. Statistically significant upregulated miRNAs are shown in green and downregulated miRNAs in red. 129 differentially regulated miRNAs were detected. Ten miRNAs were chosen for further studies (highlighted in blue) based on high fold changes, statistical significance and relevant pathways. (b, c) Microarray data for the selected upregulated (b) and downregulated (c) miRNAs were validated by qPCR. HSFs from two different human donors were used to validate the microarray results (ID 595, ID 222). The miRNA levels are shown as log2 fold changes of rF1M-WT *versus* rF1M-RGA. Values are indicated as mean values of biological triplicates with three technical replicates each ± SEM. Student's *t* test was performed to assess statistical significance (* $p < 0.05$). (d) Time course analysis (2, 4, 8 and 24 h after cell seeding on rF1M-WT or rF1M-RGA) by qPCR for the selected differentially regulated miRNAs identified in the microarray. "Time" represents the starting time point when consistent and significant differential miRNA regulation occurred. Green boxes represent the upregulated and red boxes the downregulated miRNAs upon HSFs binding to rF1M-WT.

explain why 24 h after fibrillin-1 binding, profound changes in mRNA expression can occur.

The miRNA signature is specific to RGD-mediated fibrillin-1 binding

To exclude the possibility that the mRNA and miRNA expression patterns observed by microarrays were induced by mechanical stress triggered by the atypical shape of HSFs seeded on the RGA-containing fibrillin-1 fragment (Supplemental Fig. S4A), controls with cells seeded on poly-D-lysine were included. Poly-D-lysine is a positively charged amino acid polymer widely used as an effective non-integrin attachment factor for cultured monolayer cells. HSFs seeded on poly-D-lysine-coated plates had a similar phenotypic appearance as cells seeded on rF1M-WT (Fig. 3a). Therefore, potential differences in miRNA regulation observed between HSFs seeded on poly-D-lysine and the fibrillin-1 wild-type fragment can be attributed to RGD-mediated signaling events and not to mechanical stress-induced signaling pathways. If the observed miRNA regulation patterns are simply a consequence of the differences in shape or adherence to the culture dish, then no differences in miRNA levels should be observed between HSFs seeded on rF1M-WT and poly-D-lysine. All tested miRNAs (miR-29b-1*, miR-424*, miR-503, miR-4521) upregulated upon interaction with the RGD-containing rF1M-WT relative to rF1M-RGA were also upregulated relative to poly-D-lysine (Fig. 3b, left panel). Downregulation of selected miRNAs (miR-612, miR-1208, miR-1231, miR-3185) upon interaction with rF1M-WT as compared the RGA control was even stronger (2.0- to 3.6-fold) for HSFs seeded on rF1M-WT relative to poly-D-lysine (Fig. 3b, right panel). In summary, the differential upregulation or downregulation was conserved for all tested miRNAs, demonstrating that the induction or repression of the respective miRNAs is confidently mediated by the RGD sequence in fibrillin-1.

Various extracellular matrix proteins contain an RGD cell binding site. To address specificity for the fibrillin-1 RGD site, we have produced and analyzed two fibronectin fragments encompassing either the RGD or an inactive RGA motif in the 10th fibronectin type III (FNIII-10) domain and the synergy site in the FNIII-9 domain (Supplemental Fig. S1A). As expected, FN-WT promoted cell attachment, whereas FN-RGA did not (Supplemental Fig. S4B, D). Interaction of HSFs with fibronectin resulted in both similar and distinct miRNA expression patterns compared to the interaction with fibrillin-1 (compare Fig. 3b and c). Cell adhesion to FN-WT also resulted in the upregulation of miR-29b-1*, miR-503, and miR-4521, but not of miR-424*. For the downregulated miRNAs, only miR-1208 and miR-1231 show a similar expression upon fibrillin-1 and fibronectin binding, whereas miR-612 is upregulated and miR-3185 remains unchanged when cells are ligated to fibronectin.

Fibrillin-1-induced miRNAs target mRNAs for growth factors, actin-binding proteins and integrins

Since growth factor activity, actin binding and integrin binding are three of the most relevant groups identified by the mRNA microarray, we explored the miRNA-dependent regulation of their mRNA levels. First, bioinformatics analysis using the miRanda algorithm was conducted to predict interactions between miRNAs and mRNAs [49]. Specifically, the interaction between all eight miRNAs validated by qPCR (miR-29b-1*, miR-424*, miR-503, miR-612, miR-1208, miR-1231, miR-3185 and miR-4521) and validated mRNAs relevant for growth factor activity, actin or integrin binding (*TGFB2*, *BMP2*, *CTGF*, *CYR61*, *NOV*, *AFAP1*, *CNN1*, *TAGLN*, and *ITGB3*) was assessed (Table 2). The six dysregulated mRNAs in the focal adhesion group reported in Table 1 were not in the predicted target list of the eight selected miRNAs and thus were not further analyzed. This analysis predicted some miRNAs as potent regulators of a number of potential and relevant targets, and provided a candidate list for the subsequent experimental confirmation. To validate these targets, we used the established method of overexpressing a mutant GW182 protein that normally plays an important role in miRNA-mediated gene silencing [50–52]. GW182 proteins directly interact with Argonaute proteins [53], are recruited to miRNA targets, and promote their silencing. The overexpression in the human fibroblast cell line MSU1.1 enabled the locking of miRNAs and their targets in the RISC complex. We focused on the miRNAs with three or more predicted targets, and thus, miR-424* and miR-4521 were not included in the experimental validation. The experimentally validated interactions of miR-29b-1*, miR-503, miR-612, miR-1208, miR-1231, and miR-3185 with growth factor, actin-binding proteins and integrin binding mRNAs are summarized in Table 3. In total, 17 (58%) of the 29 algorithm-based prediction of the miRNA-mRNA interactions could be validated. Experimental details are shown in Supplemental Figs. S5, S6 and S7. Five of the nine tested mRNAs (*TGFB2*, *CTGF*, *NOV*, *AFAP1*, *CNN*) were validated as targets for at least four of the six most dysregulated miRNAs. Among them, *TGFB2* is validated to be regulated by all the six tested miRNAs. These data indicate that the fibrillin-1-controlled miRNAs indeed act in these functional groups.

Fibrillin-1 and miR-503 regulate canonical TGF-β signaling

Since fibrillin-1 is involved in the regulation of TGF-β bioavailability and activity through its interaction with the LTBPs, we explored whether the interaction of fibrillin-1 with fibroblasts directly affects TGF-β signaling pathways. HSFs displayed

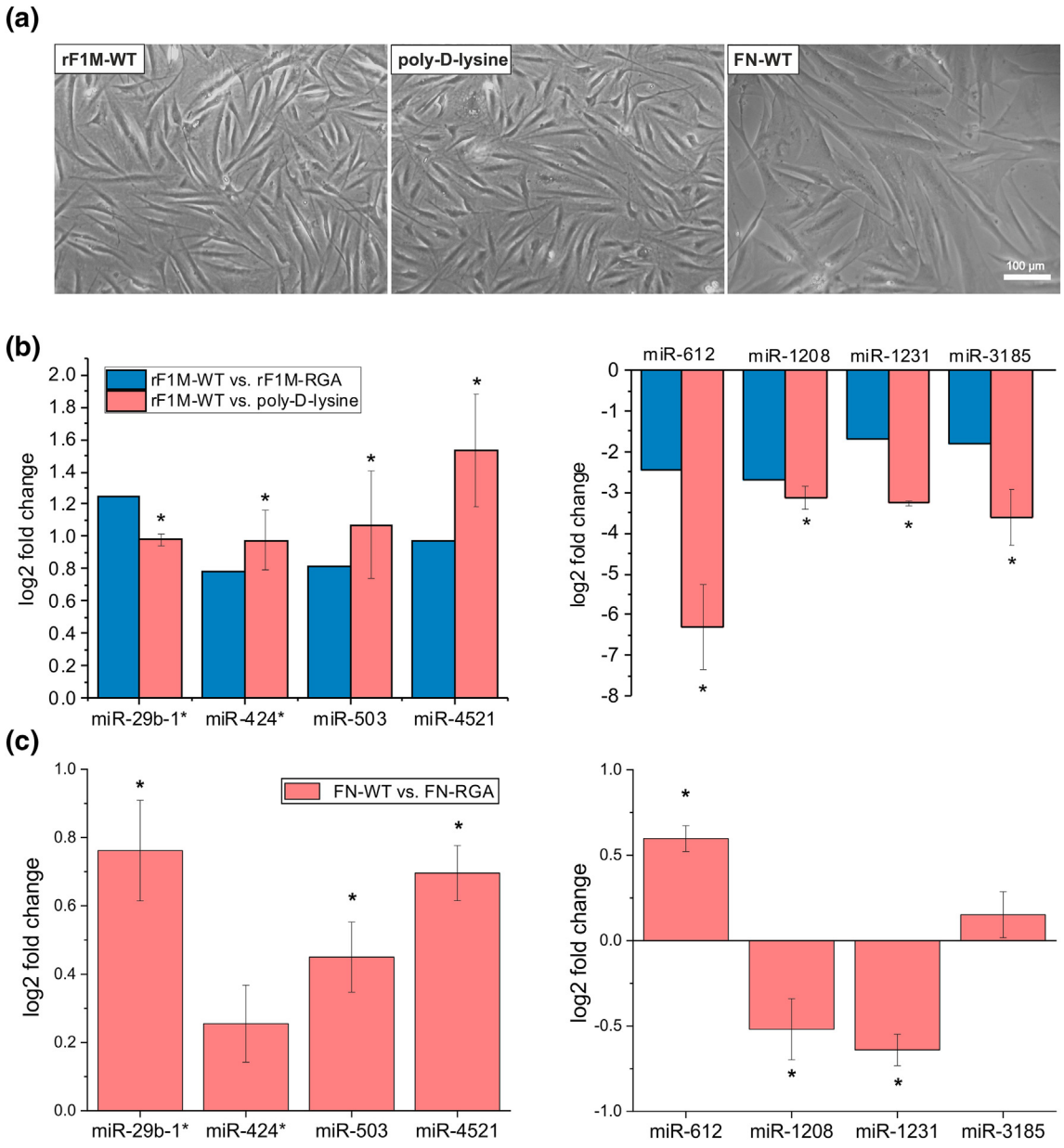

Fig. 3. Specificity of fibrillin-1 mediated miRNA regulation. (a) Light microscopic images of HSFs (ID 595) grown for 24 h on rF1M-WT, poly-D-lysine, or FN-WT-coated culture dishes as indicated. (b) qPCR analysis to determine the specificity of miRNA regulation mediated by fibrillin-1 exemplified with selected miRNAs. miRNA levels were determined for HSFs grown for 24 h on rF1M-WT *versus* poly-D-lysine-coated plates (red columns). For comparison, rF1M-WT *versus* rF1M-RGA data for 24 h are shown from the miRNA microarray in Fig. 2a (blue columns). Upregulated miRNAs in the microarrays are shown on the left panel, downregulated miRNAs on the right panel. (c) Corresponding miRNAs level were determined 24 h after HSFs interacting with FN-WT compared to FN-RGA controls. In panels b and c, the miRNA levels are shown as log2 fold changes of rF1M-WT *versus* poly-D-lysine, rF1M-WT *versus* rF1M-RGA and FN-WT *versus* FN-RGA, respectively. Values are indicated as mean values of biological triplicates with three technical replicates each ± SEM. Student's *t* test was performed to assess statistical significance (* $p < 0.05$).

differential activities of the canonical TGF-β signaling pathway, depending on the substrate they were seeded on, as evidenced by immunofluorescence staining for phosphorylated Sma- and Mad-related protein 2 (p-Smad2) (Fig. 4a). The pathway was more active 24 h after HSFs were seeded on the mutant RGA-containing fragment as shown by a stronger p-Smad2 signal intensity (149%) relative to the Tris-buffered saline (TBS) control, potentially mediated through non-integrin heparan sulfate

Table 2. Predications of interactions between miRNAs and mRNAs

Target mRNA	miRNA							
	miR-29b-1* ↑	miR-424* ↑	miR-503 ↑	miR-612 ↓	miR-1208 ↓	miR-1231 ↓	miR-3185 ↓	miR-4521 ↑
Growth factors								
TGFB2 (transforming growth factor beta 2) ↓	++	–	+	–	++	+	–	–
BMP2 (bone morpho-genetic protein 2) ↓	++	–	–	–	–	++	++	–
CTGF (connective tissue growth factor) ↑	++	–	–	–	+	++	–	–
CYR61 (cysteine-rich protein 61) ↑	–	–	–	–	–	–	–	–
NOV (nephroblastoma overexpressed) ↓	++	–	+	–	–	+	–	–
Actin binding								
AFAP1 (actin filament associated protein 1) ↑	+	++	+	+	+	+	+	–
CNN1 (calponin 1) ↑	–	–	+	+	+	–	–	–
TAGLN (transgelin) ↑	+	–	–	+	–	–	–	–
Integrin binding								
ITGB3 (integrin beta 3) ↓	–	+	–	++	+	+	+	–

Bioinformatic prediction of interactions and regulation between miRNAs and mRNAs. The miRanda algorithm was used to assess the probability of interaction between a certain miRNA and an mRNA (microrna.org) [49]. ++ indicates highly probable interactions, + interactions with low probability, and – no predicted interactions. Upregulation of miRNAs and mRNAs as determined by the microarrays is indicated by up-pointing arrows, and downregulation by down-pointing arrows.

binding sites present on the rF1M constructs (Supplemental Fig. S1A). Contrary, interaction with the wild-type fibrillin-1 fragment led to reduced TGF-β signaling to about 55% of the control after 24 h. This correlates with downregulated *TGFB2* mRNA levels upon integrin interaction with rF1M-WT, as observed in the microarray (Fig. 1c). TGF-β1 control treatment for 24 h induced the strongest activation (197% of the control) of the TGF-β signaling pathway. In summary, fibrillin-1 interaction with HSFs controls the canonical TGF-β pathway by dampening its activity.

Since all tested fibrillin-1-controlled miRNAs target *TGFB2* mRNA (Table 3), we performed functional analysis on the TGF-β signaling pathway. The role of miR-503 was of particular interest because the upregulation of miR-503 in HSFs on rF1M-WT correlates with the downregulation of *TGFB2* mRNA in the microarray and qPCR. HSFs seeded on TBS control wells were transfected with miR-503 mimics and p-Smad2 activity was analyzed after 48 h by immunofluorescence (Fig. 4b). A significant reduction in the p-Smad2 intensity to 64% was observed when miR-503 was overexpressed

Table 3. Experimentally validated interactions between miRNAs and mRNAs

Target mRNA	miRNA					
	miR-29b-1* ↑	miR-503 ↑	miR-612 ↓	miR-1208 ↓	miR-1231 ↓	miR-3185 ↓
(a) Growth factors						
TGFB2 (transforming growth factor beta 2) ↓	+	+	+	+	+	+
BMP2 (bone morphogenetic protein 2) ↓	–	–	–	–	–	–
CTGF (connective tissue growth factor) ↑	+	–	+	+	+	–
CYR61 (cysteine-rich, angiogenic inducer 61) ↑	+	–	+	–	–	–
NOV (nephroblastoma overexpressed) ↓	+	+	+	–	–	+
(b) Actin binding						
AFAP1 (actin filament associated protein 1) ↑	+	+	–	+	+	–
CNN1 (calponin 1) ↑	+	+	+	–	+	–
TAGLN (transgelin) ↑	+	–	–	–	+	–
(c) Integrin binding						
ITGB3 (integrin beta 3) ↓	+	–	–	+	–	–

The interactions between miR-29b-1*, miR-503, miR-612, miR-1208, miR-1231 and miR-3185 with mRNAs were experimentally validated. Student's *t* test was performed to assess statistical significance (* $p < 0.05$). The overview table indicates experimentally validated interactions (+) and no interactions (–) between the miRNAs and the respective mRNAs. Upregulation of miRNAs and mRNAs as determined in the microarrays is indicated by up-pointing arrows, and downregulation by down-pointing arrows.

compared to the non-transfected control. This explains the situation when HSFs are seeded on rF1M-WT, resulting in upregulation of miR-503 and downregulation of p-Smad2 dependent TGF-β activity. In conclusion, miR-503 contributes to the reduced TGF-β signaling observed upon binding of HSFs to fibrillin-1.

miR-612 and miR-3185 regulate fibrillin-1-mediated focal adhesion formation

Since focal adhesion formation is one of the important downstream events after fibrillin-1 integrin binding to fibroblasts [20], the focal adhesion kinase (FAK) activity was assessed by immunofluorescence for phosphorylated FAK. To facilitate this analysis, HSFs were seeded on either rF1M-WT or rF1M-RGA coated Y-shaped micropatterns (1600 μm^2) that provided a defined area and shape for the cells to attach (Fig. 5a). HSFs seeded on rF1M-WT frequently occupied the entire available area, whereas cells seeded on the rF1M-RGA did often not occupy the entire area. The number, average area and total area of focal adhesions per cell were significantly higher in HSFs seeded on rF1M-WT as compared to the rF1M-RGA control (Table 4).

Since rF1M-WT interaction with HSFs resulted in upregulation of miR-29b-1* and miR-503, and downregulation of miR-612, miR-1208, miR-1231 and miR-3185 (see Fig. 1), we transfected HSFs with miRNA mimics and inhibitors, respectively, to analyze whether these miRNAs are mediators of focal adhesion formation (Fig. 5b and c). miR-29b-1* overexpression did not change the number of focal adhesions per cell, but led to a significantly decreased average size. miR-503 overexpression resulted in significantly lower number and average size of focal adhesions (Fig. 5b). Thus, miR-29b-1* and miR-503 cannot be mediators of the fibrillin-1-promoted focal adhesion formation. For miR-612, miR-1208, miR-1231, or miR-3185, only inhibition of miR-612 showed a significant increase in both number and average size of focal adhesions, whereas inhibition of miR-3185 resulted in an increased average size of focal adhesions (Fig. 5c). Inhibition of miR-1208 decreased the focal adhesion number.

This result indicates that miR-612 and miR-3185 mediate the fibrillin-1-induced focal adhesion formation. To further prove this possibility, miR-612 or miR-3185 was overexpressed in HSF seeded on rF1M-WT (Fig. 6a), demonstrating that the miR-3185 mimic could downregulate the total area of focal adhesion per cell. Furthermore, rescue experiments to inhibit miR-612 or miR-3185 on HSF seeded on rF1M-RGA (Fig. 6b) showed that the miR-612 inhibitor can rescue the total area of focal adhesion per cell.

In conclusion, miR-612 and miR-3185 contribute to the fibrillin-1 mediated regulation of focal adhesion formation in HSFs.

Discussion

miRNAs are key regulators of gene expression of cellular processes, including the regulation of the extracellular matrix. However, how extracellular matrix proteins regulate the expression of miRNAs and associated downstream cell functions is currently very little explored. Many extracellular matrix proteins interact with cells via RGD-dependent integrin receptors. Here, we use fibrillin-1 as a model protein because of its importance in tissue and organismal development. We and others have shown that the RGD sequence in fibrillin-1 provides the molecular basis for cell adhesion via integrin $\alpha_5\beta_1$, $\alpha_v\beta_3$ and $\alpha_v\beta_6$ [16–20]. In the present study, we provide for the first time a comprehensive analysis of how fibrillin-1–integrin interaction regulates miRNA expression and downstream cell function using dermal fibroblasts as a model system. Furthermore, our study significantly extends the repertoire of how miRNAs act in several miRNA-mediated regulatory pathways, most importantly the TGF-β signaling pathway and focal adhesion formation.

Integrin-mediated fibrillin-1 interaction with dermal fibroblasts resulted in profound changes of mRNA and miRNA expression patterns. Global microarray analysis revealed differential expression of 520 mRNAs and 129 miRNAs after 24 h of interaction of fibroblasts with fibrillin-1. Independent pathway analysis for mRNA and miRNA expression demonstrated significant overlaps. The differentially expressed mRNAs and miRNAs act together in signaling pathways mediated by TGF-β, Wnt, MAPK, or Hedgehog, and in pathways for cytoskeletal organization. These are pathways hitherto not directly associated with the interaction between fibrillin-1 and cells, and they are potentially involved in the pathogenesis of some of the fibrillin-1 associated disorders. None of the identified miRNAs have been described previously in regard to fibrillin-1 mediated cell signaling.

We have analyzed the specificity of fibrillin-1-regulated miRNA expression in two ways. First, we tested whether the different cell shapes of HSFs seeded on rF1M-WT compared to rF1M-RGA could cause the differential miRNA regulation. However, we have observed similar patterns of upregulated or downregulated miRNAs when HSFs were seeded on rF1M-WT compared to either rF1M-RGA or to cells seeded on poly-D-lysine, a substrate that HSFs readily attach to and spread on, excluding this possibility. Second, we have analyzed the specificity for the RGD binding site in fibrillin-1. Analyzing a selected set of miRNAs with HSFs seeded on a fibronectin control fragment containing the RGD sequence in the 10th type III domain revealed similarities and differences compared to the rF1M-RGD-seeded HSFs. While the overall pattern was similar, miR-612 and miR-3185, for example, were downregulated in cells seeded on rF1M-WT and either upregulated (miR-612) or

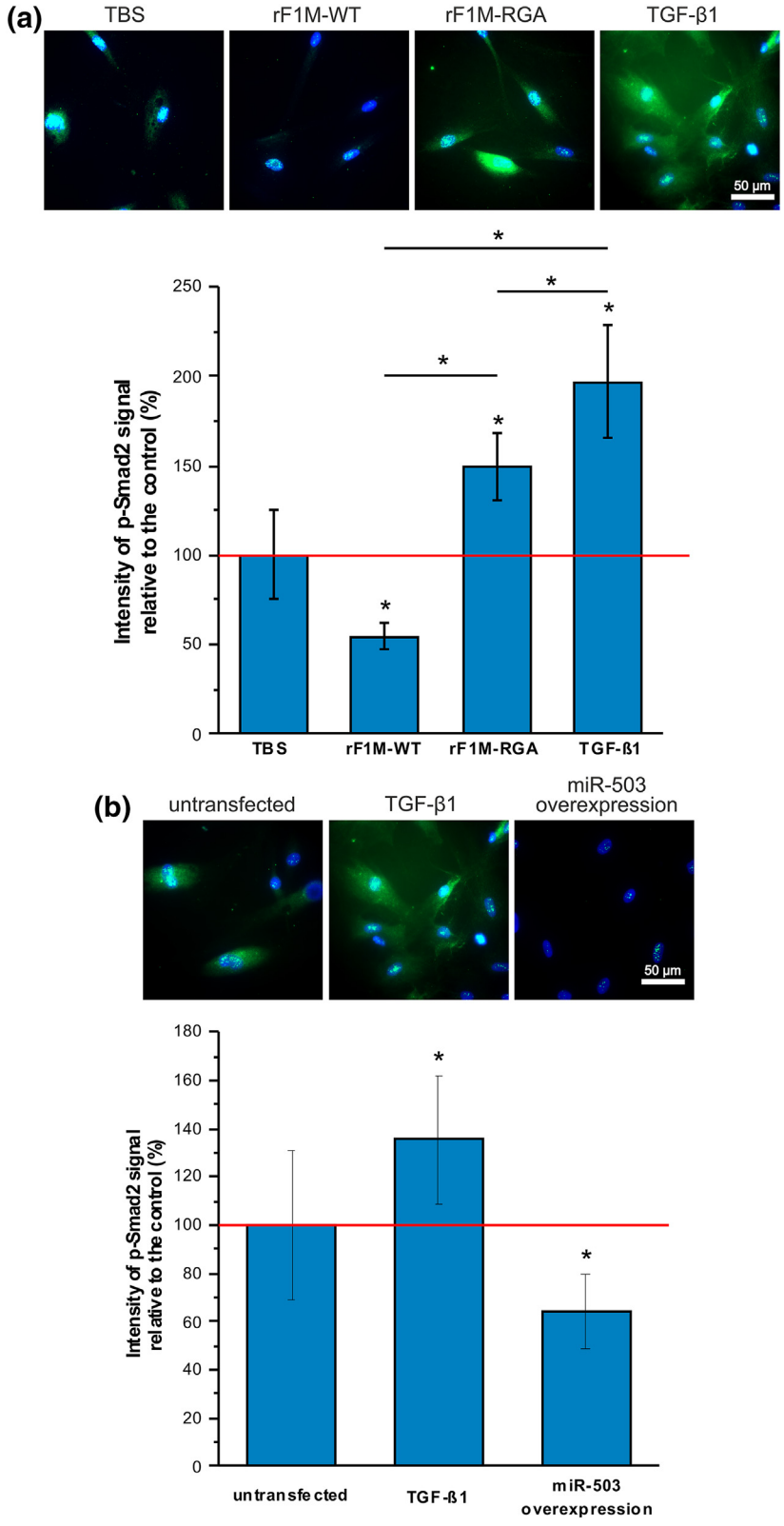

Fig. 4. TGF-β signaling upon interaction with fibrillin-1 and overexpression of miR-503. (a) Immunofluorescence staining for p-Smad2 was conducted at 24 h after cell seeding. 10,000 HSFs (ID 595) were seeded per well of an 8-well chamber slide coated with rF1M-WT or rF1M-RGA at 25 µg/mL or TBS buffer as a control. As a positive control, cells were treated with TGF-β1 (5 ng/mL) for 24 h. Representative images for each condition are shown. The intensity of the p-Smad2 signal 24 h after cell seeding was quantified in the lower panel. Each condition was analyzed in biological duplicates. Five different images were recorded for each duplicate. Untreated cells seeded on TBS control wells were used as reference set to 100% for comparison with all other conditions (red line). Statistical analysis was performed using Student's *t* test (* $p < 0.05$). Statistical significance is indicated for each value relative to the control reference, indicated by asterisks above the error bars. Statistically significant differences between the rF1M-WT, rF1M-RGA and TGF-β1 samples are indicated by asterisks above horizontal lines. (b) Immunofluorescence staining for p-Smad2 was conducted 48 h after cell seeding under conditions as in panel a. Cells were transfected with miR-503 mimics at the time of seeding or treated with TGF-β1 (5 ng/mL) for 48 h. An untransfected control was included as indicated. Representative images for each condition are shown. Quantification of the intensity of the p-Smad2 signals is shown in the lower panel. Each condition was analyzed in biological duplicates. Five different images were recorded for each duplicate. Untransfected cells seeded on TBS control wells were used as a reference for comparison with the other conditions (100%; red line). Statistical analysis was performed using Student's *t* test (* $p < 0.05$).

unchanged (miR-3185) in cells seeded on fibronectin. While we have not experimentally addressed the molecular cause for these protein-specific responses, it is possible that they originate from the following molecular aspects. Fibrillin-1 and fibronectin RGD sites share binding with $\alpha_5\beta_1$ and $\alpha_v\beta_3$ integrins expressed on fibroblasts. For fibrillin-1, binding to $\alpha_5\beta_1$ integrin was reported of relative low affinity, whereas it interacts with fibronectin with high affinity [19,54]. Different synergy sites upstream of the RGD sites in both proteins may also contribute to the modulation of the downstream signaling [20,55], and fibronectin may involve additional RGD-binding integrins that are not shared with the known set of fibrillin-1 interacting integrins [56]. In addition, glycosylation patterns in close vicinity to the RGD site in fibrillin-1 and fibronectin may modulate specificity. In rF1M constructs, there are two predicted N-linked glycosylation sites located relatively close to the RGD site (one in the TB4 domain and one in the preceding cbEGF domain), whereas N-linked glycosylation is not predicted for the fibronectin constructs employed in this study. This was one of the reasons why we could utilize a bacterial expression system to produce the fibronectin constructs. On the other hand, both proteins contain several predicted O-linked glycosylation sites in close vicinity of the respective RGD sites [57]. Here, we cannot answer the question whether or not those sites would contribute to the observed specificities in eliciting miRNA responses. This will require recombinant expression of the fibronectin constructs in glycosylation-competent mammalian cells.

It is well documented that fibrillin-1 is involved in the regulation of TGF-β bioavailability via its interaction with several LTBPs [32,58]. Here, we demonstrate an additional mechanism how fibrillin-1 controls TGF-β. Fibrillin-1 interaction with HSFs controls the canonical TGF-β pathway by dampening p-Smad2 activity. One of the miRNAs that are upregulated when fibrillin-1 interacts with HSFs is miR-503, and overexpression of miR-503 in HSFs reduces p-Smad2 activity. We also have determined that *TGFB2* mRNA is a direct target of miR-503 (Table 3), which will be downregulated when miR-503 is elevated. Potentially, miR-503 also targets other critical mRNAs in the TGF-β signaling pathway in fibroblasts, not tested in the present study. These data extend the current concepts how fibrillins are involved in the regulation of TGF-β, demonstrating a regulatory mechanism via integrin-mediated and miRNA-dependent gene expression.

Previous *in vivo* studies demonstrated that heterozygous mice with an RGD to RGE substitution in fibrillin-1 (*Fbn1*$^{RGE/+}$) displayed diffuse skin fibrosis including increased deposition of collagen and microfibrils, similar to stiff skin syndrome patients that carry mutations in the TB4 domain [34,59]. Enhanced TGF-β bioavailability contributed to increased TGF-β activity in these mutant mice. Importantly, that study showed increased total (latent and free) TGF-β2 in the dermis of mutant mice, but no difference in free TGF-β. These findings correlate directly with our observation of *TGFB2* mRNA downregulation when HSFs interact with the wild-type fibrillin-1 fragment, and therefore upregulation when HSFs are grown on the integrin binding-deficient fibrillin-1 RGA mutant. Fibroblasts from patients with systemic sclerosis showed decreased levels of miR-29a *in vitro* [59]. The miR-29 family members are known to be repressed by TGF-β and inhibit the expression of multiple matrix components in fibroblasts and suppress fibrosis [60,61]. Integrin-modulating therapies and TGF-β antagonism restored miR-29a levels in patient-derived fibroblasts [59]. miR-29a targets genes related to extracellular matrix, such as fibrillin-1, integrins, collagens and laminins [62]. Although miR-29b-1* has a different seed region compared to miR-29a and thus different targets, miR-29a and miR-29b-1* are co-expressed from the same cluster [41,63]. In the present study, we show miR-29b-1* to be significantly upregulated when HSFs bind to wild-type fibrillin-1, while miR-29b-1 remains unchanged. Furthermore, *TGFB2* mRNA, which we have experimentally determined as a direct target of miR-29b-1*, and p-Smad2-dependent TGF-β signaling are also kept at a low level when HSFs binds to rF1M-WT. These results suggest that miR-29b-1* is involved, in addition to miR-503, in fibrillin-1 mediated dampening of TGF-β activity. However, this likely occurs on a network level, as overexpression of miR-29b-1* alone in HSFs did not result in reduced TGF-β activity (not shown).

Integrin interaction with extracellular proteins stimulates the assembly of focal adhesions at the cell membrane. The integrin/focal adhesion complex serves as a crucial element for mechanotransduction [64] and is essential for the activation of TGF-β [65]. Focal adhesion formation triggered by RGD-containing fibrillin-1 fragments was previously shown for keratinocytes mediated through integrin $\alpha_v\beta_6$ [19]. Bax *et al.* [20] reported that the TB5-cbEGF25 domains support the formation of focal adhesions. However, the contribution of the RGD site alone to focal adhesion formation was not tested. HSFs seeded on the rF1M-WT developed significantly more focal adhesions and can spread better than HSFs seeded on the rF1M-RGA control. However, HSFs seeded on the rF1M-RGA fragments still develop focal adhesions to some extent (Fig. 5a). It is possible that the described supporting role of the heparin/heparan sulfate binding site located in TB5 does not entirely depend on the interaction of integrins with the RGD site in TB4 [20].

Regardless of whether or not non-RGD sites in fibrillin-1 have independent separate roles in focal adhesion formation, we have identified two miRNAs, miR-612 and miR-3185, as important regulators for fibrillin-1-mediated focal adhesion formation for the following reasons. These miRNAs are both

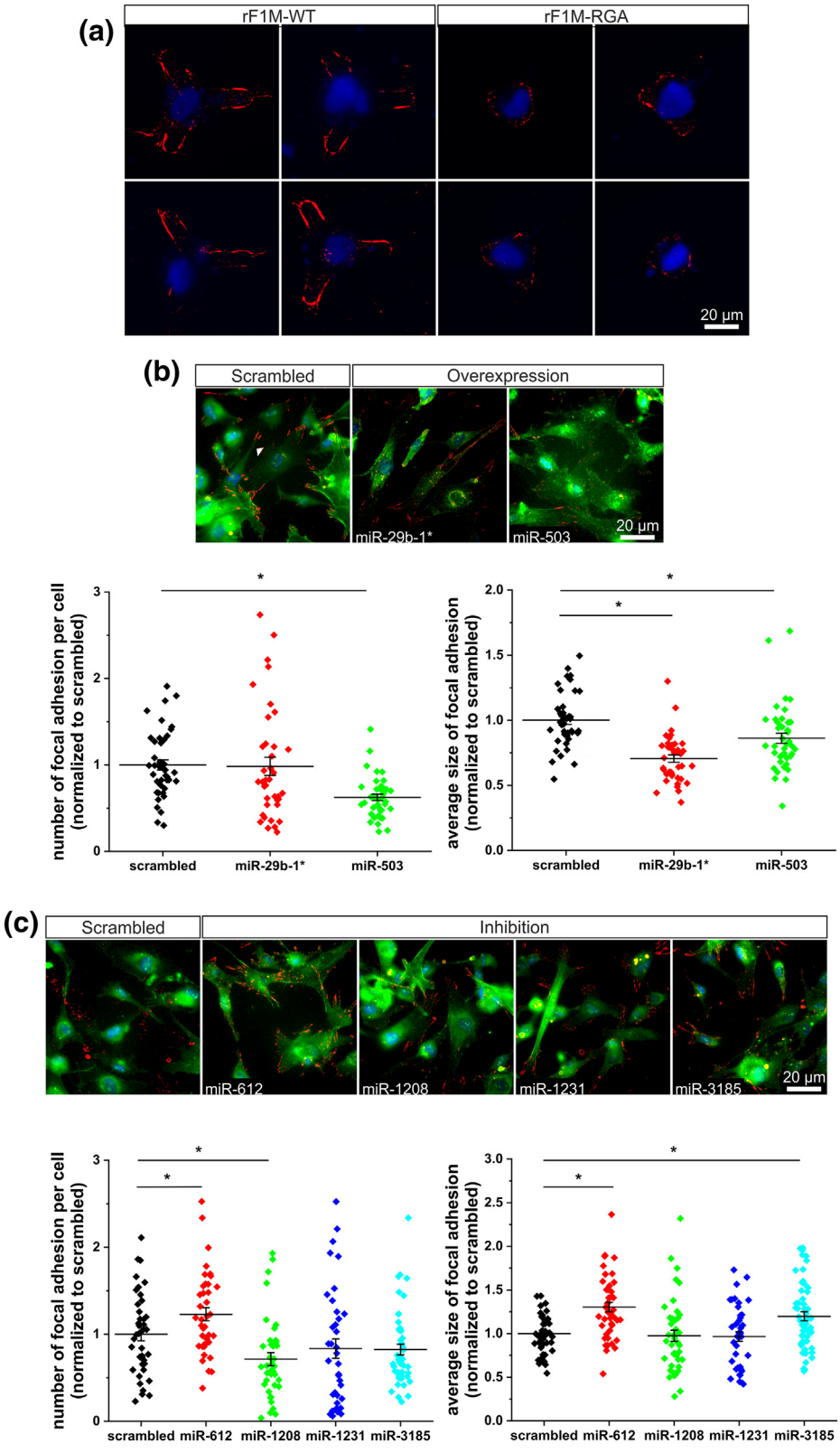

Fig. 5 (*legend on next page*)

Table 4. Quantification of focal adhesion (FA) formation of HSFs seeded on rF1M-WT and rF1M-RGA coated Y-shaped micropatterns

	Number of FAs per cell	Average area of FA	Total area of FAs per cell
rF1M-WT	94 ± 37	0.74 ± 0.14 μm^2	68.01 ± 25.90 μm^2
rF1M-RGA	52 ± 23	0.55 ± 0.10 μm^2	29.76 ± 16.43 μm^2
p Value	3.80E−05	5.02E−06	3.20E−07

The data are presented as average ± SD. *p* values were calculated comparing rF1M-WT *versus* rF1M-RGA using the two-sample *t* test. Number of cells analyzed: 32 cells for rF1M-WT and 20 cells for rF1M-RGA.

downregulated when HSFs are seeded on rF1M-WT. miR-612 and miR-3185 inhibition in HSFs led to significantly more focal adhesions or more developed focal adhesions. Rescue experiments showed that focal adhesion formation in HSFs could be enhanced by miR-612 inhibition in HSFs grown on rF1M-RGA, or inhibited by miR-3185 overexpression in HSFs seeded on rF1M-WT. Calponin 1, which we have validated as a target for miR-612, is a myofibroblast and smooth muscle cell marker [66]. The level of calponin 1 mRNA was elevated in the microarray and qPCR when HSFs were grown on rF1M-WT, concomitant with the downregulation of miR-612. This indicates that HSFs seeded on fibrillin-1 have differentiated into smooth muscle α-actin expressing myofibroblast, which promotes focal adhesion maturation [67]. The regulation of calponin 1 by miR-612 could be one of the underlying mechanisms of HSF focal adhesion assembly regulated by extracellular fibrillin-1, via regulating myofibroblast differentiation.

Virtually no information is available in the literature about the function of miR-3185. Despite the fact that we were not able to identify and validate a target for miR-3185 in the actin-binding group or the focal adhesion group that is dysregulated in the mRNA microarray more than 2-fold, we demonstrate here that it acts in the pathway of fibrillin-1-regulated focal adhesion formation as shown by the cell culture rescue experiments. Re-inspection of the mRNA microarray data comparing HSFs seeded on rF1M-WT *versus* rF1M-RGA using a lower threshold (>1.4-fold change) revealed two possible candidates involved in focal adhesion formation/stability, talin 1 (1.45-fold upregulated) and vinculin (1.53-fold upregulated). Both mRNAs are predicted targets of miR-3185 using TargetScan. Although the relative changes are low, collaboratively, these two targets could potentially account for the regulation of focal adhesions [68].

In summary, the present study shows that interaction of fibroblasts with the RGD site in fibrillin-1 controls the expression of many mRNAs and miRNAs in pathways relevant to fibrillin function. We predict similar mechanisms for assembled microfibrils, as they retain their ability to interact with integrins α5β1 and αvβ3 [18]. We have identified 28 new mRNA targets for several of the fibrillin-1-regulated miRNAs and have shown that some are involved in the regulation of TGF-β signaling and in focal adhesion formation. This work shows that matrix proteins (fibrillin-1 and fibronectin) can regulate the levels of miRNAs through their interaction with integrins. These findings may proof relevant in the future for some connective tissue disorders that are caused by fibrillin-1 deficiencies, including stiff skin syndrome and Marfan syndrome.

Materials and Methods

Generation of recombinant expression plasmids

Full-length fibrillin-1 has the propensity to aggregate and is thus difficult to purify [69]. Due to the modular domain organization, smaller correctly folded fibrillin-1 fragments are often used to study the functional properties of different regions in fibrillin-1 [10,69–72]. To recombinantly produce a central human fibrillin-1 fragment containing the RGD integrin binding site and the synergy site, but not the N-terminal and C-terminal self-interaction sites, the following expression plasmids were generated. A DNA sequence coding for human

Fig. 5. Consequences of fibroblast interaction with fibrillin-1 and of miRNA modulation on focal adhesion formation. (a) Immunofluorescence staining of phosphorylated FAK (red) was conducted 24 h after HSF seeding on 1600 μm^2 Y shape micropattern (Cytoo) coated with either rF1M-WT or rF1M-RGA at 25 μg/mL. Representative images for each condition are shown. (b) Immunofluorescence staining for actin (green) and phosphorylated FAK (red) was conducted after 48 h after HSF seeding on non-coated chamber slides. For each condition, cells were either transfected with miRNA mimics for miR-29b-1* and miR-503 or inhibitors for miR-612, miR-1208, miR-1231 and miR-3185 at the time of seeding. A scrambled control was included. Representative images for each condition are shown. Quantification of the number (left panels) and average sizes (right panels) of focal adhesion per cell normalized to the respective scrambled control is shown below each immunofluorescence panel. A total of 60 images from biological triplicates were quantified. Each bar represents the mean ± SEM. Statistical analysis was performed using Student's *t* test (* $p < 0.05$).

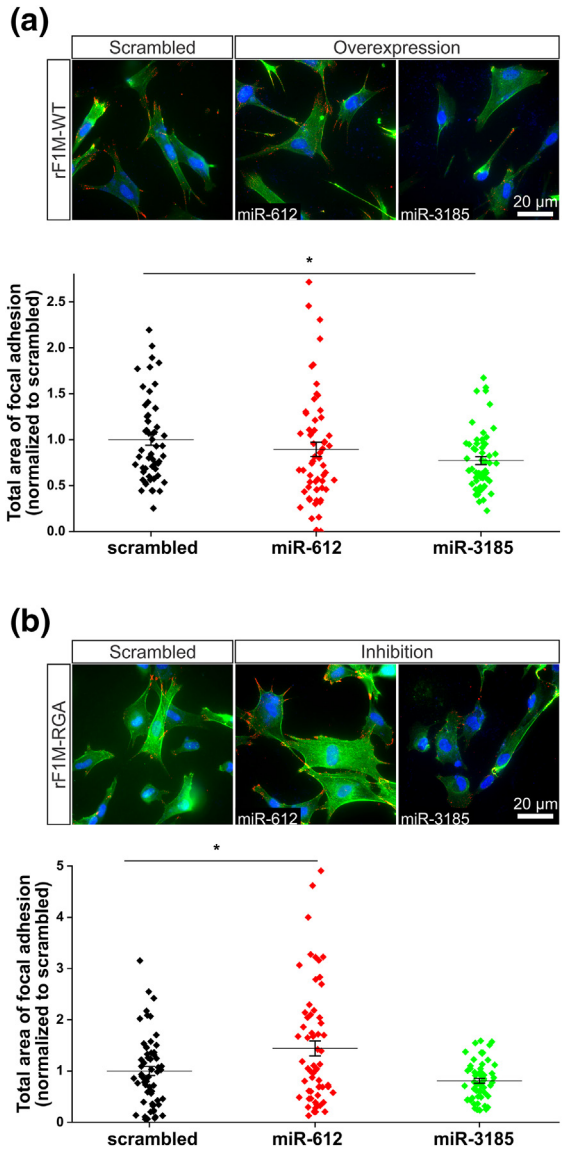

Fig. 6. Rescue experiments of fibrillin-1-regulated miRNA on focal adhesion formation. (a) HSFs seeded on rF1M-WT-coated chamber-slides (as described as Fig. 5) were transfected with miR-612 or miR-3185 mimics, or with a scrambled miRNA as control. (b) HSFs seeded on rF1M-RGA coated slides were transfected with inhibitors of miR-612, miR-3185 or a scrambled control. For both panels a and b, immunofluorescence staining (top panels) for phosphorylated FAK (red) and actin (green) was conducted after 48 h, and the phosphorylated FAK signals were quantified (bottom panels) as total area of focal adhesions per cell normalized to the respective scrambled control. The data represent three independent experiments with HSFs from two different donors and different passage numbers. A total of 60 images for each condition were quantified. Each bar represents the mean ± SEM. Statistical analysis was performed using Student's *t* test (* $p < 0.05$).

fibrillin-1 domains cbEGF10 to cbEGF31 including an N-terminal signal peptide from the BM40 protein and a C-terminal octa-histidine tag were prepared with appropriate oligonucleotides based on the pCEPSP-rF18H plasmid described previously [73]. The resulting plasmid pCEPSP-rF1M-WT codes for a protein (rF1M-WT) with the sequence APLAD^{910}-Q^{2054}GRAWSHPQFEKGASGEHHHHHHHHH (human fibrillin-1 sequence is underlined). To generate a plasmid that harbors an inactive integrin binding site, the pDNSP-rFBN1-RGA plasmid described previously [26], was amplified by PCR and a *PmlI* × *NotI* restricted fragment was subcloned into pCEPSP-rF1M-WT, resulting in plasmid pCEPSP-rF1M-RGA. This plasmid codes for a protein (rF1M-RGA) identical to rF1M-WT except an D^{1543}A mutation in the RGD motif.

Full-length fibronectin contains multiple integrin binding sites. To exclude integrin binding sites other than the RGD in the 10th type III domain and to include the synergy site in the 9th type III domain, recombinant expression plasmids were produced coding for the amino acid sequence from the 8th to 11th type III domain (A^{1356}-T^{1720}) with either the wild-type RGD sequence (FN-WT) or a mutant RGA (FN-RGA). This region of fibronectin does not include any disulfide bonds or N-linked glycosylation sites. To facilitate identification and purification of the expressed recombinant fragments, the expression plasmids were designed to include sequences coding for a V5 tag and a hexa-histidine tag (5′-GGTAAGCC TATCCCTAACCCTCTCCTCGGTCTCGATTC TAC-3′) inserted after the 11th type III domain and prior to the stop codon. The recombinant cDNA was commercially synthesized as gBlocks (Integrated DNA Technologies) and inserted into the pET-22b bacterial expression plasmid using Gibson Assembly (New England Biolabs). The correct sequence of all expression plasmids was validated by Sanger sequencing.

Production of recombinant proteins

Recombinant fibrillin-1 fragments were produced as secreted proteins in human embryonic kidney 293 (HEK293)-Epstein–Barr virus nuclear antigen (EBNA) cells (Invitrogen) to ensure proper disulfide bond formation and glycosylation. The pCEPSP plasmid vectors to express the recombinant fibrillin-1 fragments (rF1M-WT and rF1M-RGA) were transfected into HEK293-EBNA for episomal expression. Hygromycin B (250 µg/mL; Wisent) in cell culture medium was used to select and maintain the transfected population of HEK293-EBNA cells. The transfected HEK293-EBNA cells were cultured to confluency in triple-layer flasks (Thermo Fisher Scientific) in standard Dulbecco's modified Eagle's medium (DMEM) cell culture medium (Wisent), supplemented with 10% fetal bovine serum (Wisent). After the cells reached confluency, they were washed with 20 mM 4-(2-hydroxyethyl)-1–1-

piperazine-ethanesulfonic acid, 150 mM NaCl and 2.5 mM $CaCl_2$ (pH 7.4) to remove serum proteins, and cultured in serum-free DMEM medium to produce conditioned medium containing the secreted proteins.

The fibronectin recombinant fragments were produced in *Escherichia coli*, which was feasible due to the absence of disulfide-bonds and N-linked glycosylation in the recombinant proteins. The recombinant pET-22b plasmids were amplified in NEB-5α (*recA1* negative; New England Biolabs). For protein production, the plasmids were transformed into BL21 (DE3) cells (Thermo Fisher Scientific). IPTG (2 mM) was used to induce protein expression when the culture medium reached ~0.6–0.8 optical density at 600 nm.

Purification of recombinant proteins

The recombinant fibrillin-1 and fibronectin fragments were chromatographically purified to homogeneity in a two-step protocol as described previously [74]. Briefly, the histidine-tagged recombinant fragments were first purified by immobilized metal affinity chromatography using an increasing imidazole gradient for elution. The eluted recombinant fragments were further purified in a second step by gel filtration chromatography (Superose 12). The BCA protein assay kit (Thermo Fisher Scientific) was used to determine the concentration of the purified proteins. The recombinant fragments were analyzed by gel electrophoresis and Coomassie Blue staining under reducing and non-reducing conditions showing the expected molecular masses (Supplemental Fig. S1B). Typical yields were ~1 mg/L cell culture medium for the fibrillin-1 fragments and ~0.65 mg/L culture medium for the fibronectin fragments.

Cell culture

Human skin fibroblasts

HSFs were isolated from the foreskin of healthy boys (2 to 5 years of age), following a standard circumcision procedure. This procedure was approved by the Montreal Children's Hospital Research Ethics Board (PED-06-054), and written consent of the patient's parents was obtained. Cells were cultured in DMEM, supplemented with 10% v/v fetal bovine serum, 100 μg/mL penicillin, 100 μg/mL streptomycin and 2 mM glutamine (Wisent) at 37 °C in a 5% CO_2 atmosphere. HSFs from two human donors were used between passages 4 and 8 throughout this study. For all experiments, ID 595 was used, and some experiments additionally included ID 222.

Prior to seeding HSFs for an experiment, the cells were serum-starved to remove all growth factors and other components in fetal bovine serum, as their presence might have interfered with cell signaling pathways. For this purpose, HSFs were washed twice with phosphate-buffered saline and thereafter kept on serum-free culture medium (DMEM with supplements) for 24 h. Cell culture plates or chamber slides were coated with the fibrillin-1 fragments rF1M-WT and rF1M-RGA at a concentration of 25 μg/mL in TBS overnight. This concentration was determined as optimal in promoting cell adhesion in a real-time cell attachment assay with increasing coating concentrations (Supplemental Fig. S3). For some experiments, cell culture plates or chamber slides were coated with poly-D-lysine (100 μg/mL; Sigma), recombinant fibronectin fragments FN-WT and FN-RGA (25 μg/mL), or the culture medium was supplemented with TGF-β1 (5 ng/mL; PeproTech) as further controls.

For trypsinization, the HSFs were washed twice with phosphate-buffered saline and incubated with 0.25% trypsin–EDTA (Wisent) for exactly 3 min. Serum-free medium was added to the dissociated cells and the cell suspension was spun down for 5 min at 1200× g. The cell pellet was resuspended in serum-free medium and centrifuged for 5 min at 1200× g. The short incubation time with trypsin and the two centrifugation steps ensured limited enzymatic activity of trypsin under serum-free conditions to minimize proteolytic degradation of cell surface receptors. After coating, the plates were washed twice with TBS, and HSFs were seeded in serum-free media with supplements. Light microscopic images of HSFs were recorded using a PowerShot A640 digital camera (Canon).

MSU-1.1 cells

The experimental validation of interactions between miRNAs and mRNAs requires efficient transfection of two vectors together with miRNA mimics, which can be achieved with cell lines. We tested MSU-1.1, an HSF cell line [75] by real-time qPCR for its mRNA expression pattern of relevant target genes compared to primary fibroblasts. Generally, the expression of the tested target mRNAs was similar to the expression by primary fibroblasts. Therefore, MSU-1.1 fibroblasts were utilized for the experimental miRNA target validation. The MSU-1.1 cells were cultured under conditions as described for primary fibroblasts.

Electric cell substrate impedance sensing

Electric-cell substrate impedance sensing (ZTheta, Applied Biophysics) is a biophysical method to electronically monitor cell attachment and spreading in real-time [76]. As the cells attach to the coated protein, a change in impedance is measured to analyze cell attachment in real-time. Forty thousand HSFs were seeded per well in serum-free DMEM. The impedance was monitored over 6 h. All measurements were performed at a frequency of 32,000 and 64,000 Hz. To determine the optimal protein coating concentration for subsequent cell attachment and

spreading assays, a concentration series from 0 to 50 μg/mL rF1M-WT or FN-WT was used to coat 96W20idf plates (Applied Biophysics) overnight at 4 °C (Supplemental Fig. S3). Coating concentration (25 μg/mL) produced optimal cell binding for both recombinant fragments, and thus, this coating concentration was used for the experiments in this study.

RNA extraction

Total RNA was extracted from HSFs at various time points to study miRNA and mRNA levels by microarray and real-time quantitative polymerase chain reaction (qPCR). Total RNA includes miRNAs and mRNAs, and the extraction was performed using the miRNeasy Mini Kit (Qiagen) according to the manufacturer's instructions. One million HSFs were seeded on 10 cm in diameter cell culture dishes (Sarstedt) to ensure sufficient RNA yields.

Microarray analysis

Microarray analysis was performed for miRNAs and mRNAs using miRNA 3.0 and Human Gene 2.0 chips from Affymetrix, respectively. The miRNA 3.0 chips contained 19,724 probe sets from 153 different organisms, including 1733 human mature miRNA and 1658 human pre-miRNA probe sets. This covers all miRNA sequences in the miRNA database miRBase (Release 17, April 2011). The Human Gene 2.0 chips cover 30,654 human mRNA probe sets. The microarray analysis including RNA quality control, complementary DNA (cDNA) preparation and labeling and the actual array were conducted at the Genome Quebec Innovation Centre at McGill University. RNA samples were prepared after 24 h of interaction between HSFs and the recombinant fibrillin-1 fragments rF1M-WT and rF1M-RGA. The same RNA samples were submitted in biological quadruplicates for the miRNA and mRNA microarray analysis. The raw data from the microarrays were normalized and quality control was performed using the Expression Console software (Affymetrix). The Transcriptome Analysis Console software (Affymetrix) was applied to perform statistical tests for differential expression of expressed genes and to visualize fold changes of miRNAs and mRNAs. Normalized intensities from rF1M-WT and rF1M-RGA were compared using one-way ANOVA. After executing ANOVA, multi-testing correction was performed using the Benjamini–Hochberg FDR-controlling procedure for all the expressed genes [77]. All p values indicated refer to FDR-adjusted p values.

The microarray data for this study have been submitted to the NCBI's Gene Expression Omnibus database https://www.ncbi.nlm.nih.gov/geo [78,79] and are accessible through GEO Series accession number GSE82085.

To determine common pathways in which genes are controlled by the differentially regulated miRNAs, pathway analysis was conducted using the DIANA miRPath v.2.0 tool [48]. This bioinformatics tool searches the predicted target genes of the identified, differentially regulated miRNAs and analyzes their combinatorial effects in KEGG, a database resource for biological pathways. The DAVID Bioinformatics Resources 6.7 (https://david.ncifcrf.gov/) [80] allows searches of molecular functions of differentially expressed mRNAs to determine enriched themes and relevant KEGG pathways.

Quantification of miRNA and mRNA

For reverse transcription of miRNAs, the miScript II RT kit (Qiagen) was used, according to the manufacturer's instructions. One microgram of total RNA was typically used for reverse transcription, if not limited by a low RNA yield. For reverse transcription of mRNAs, the Super Script III First-Strand Synthesis System for RT-PCR (Life Technologies) was used as detailed in the manual. One microgram of total RNA was used, if RNA yield was sufficient.

For the quantification of miRNAs, real-time qPCR was performed using the miScript SYBR Green PCR Kit according to the manufacturer's instructions (Qiagen). miScript Primer Assays were obtained from Qiagen for human miR-29b-1* (cat. no. MS00009289), miR-424* (cat. no. MS00009688), miR-503 (cat. no. MS00033838), miR-612 (cat. no. MS00005047), miR-1208 (cat. no. MS00014196), miR-1231 (cat. no. MS00031290), miR-1914* (cat. no. MS00016548), miR-3185 (cat. no. MS00020930), miR-4443 (cat. no. MS00041272) and miR-4521 (cat. no. MS00040796). RNU6 (cat.no MS00033740) and SNORD61 (cat. no MS00033705) were used as reference genes. The real-time cycler (Applied Biosystems, Step-One™ Real-Time qPCR system) was programmed to an initial PCR activation step for 15 min at 95 °C and 40 cycles of a three-step cycling program: (1) denaturation (94 °C for 15 s), (2) annealing (55 °C for 30 s) and (3) extension (70 °C for 34 s). Melt-curve analysis was performed after each run to determine the specificity of the detected product.

For quantification of mRNA, cDNA prepared using the Super Script III First-Strand Synthesis System was used for real-time qPCR with the SYBR Green Select Master Mix (5 μL) (Life Technologies), and 100–400 nM forward and reverse primers (Supplemental Table 1). GAPDH and RPL13A were used as reference genes. The real-time cycler was programmed to an initial PCR activation step for 2 min at 50 °C and afterward 2 min at 95 °C and 40 cycles of a three-step cycling program: (1) denaturation (95 °C for 15 s), (2) annealing (58 °C for 15 s) and (3) extension (72 °C for 1 min). Melt-curve analysis

was performed after each run to determine the specificity of the detected product.

Interaction studies between miRNAs and mRNAs

Bioinformatics prediction

Bioinformatics analysis utilizing the miRanda algorithm was conducted to predict interactions between miRNAs and mRNAs [49]. This algorithm allows searches for the complementarity between miRNAs and 3′ UTRs of mRNAs and integrates thermodynamics of the binding site as well as conservation across species. The predicted target sites were scored using a regression model, the mir support vector regression (mirSVR). mirSVR scores miRNAs according to their likelihood of mRNA downregulation. The regression model comprises features of the predicted miRNA/target site duplex, local and global context features. Local features include adenine/uracil composition near the target sites and secondary structure accessibility. Global features comprise the length of the UTR, relative position of the target sites relative to UTR ends as well as the conservation level of the block containing the target site.

Experimental validation

The well-established mirTrap system (Clontech) was used to experimentally validate predicted interactions between miRNAs and mRNAs [50–52]. The system uses a dominant-negative form of a subunit of RISC, which traps the miRNA and its mRNA targets. This mutant subunit contains a FLAG epitope (DYKDDDDK), and thus, the entire complex can be immunoprecipitated, and target mRNAs can subsequently be identified by real-time qPCR.

Transfection, lysis, immunoprecipitation and RNA isolation were performed according to the manufacturer's instructions. MSU-1.1 cells at a density of 1,500,000 cells/10 cm in diameter culture plates were used for transfection with miRNA mimics and the pMirTrap vector. The transfection efficiencies were controlled with miR-132 co-transfected with the pMirTrap Control and the pMirTrap vectors. The transfected control cells were used to analyze the fold enrichment of a fluorescent quantifiable miR-132 target coded on the pMirTrap control vector. After the immunoprecipitation, the RNA was isolated from the immunoprecipitated material bound to the anti-FLAG beads ("After IP") and from the pre-immunoprecipitation control ("Before IP") using the NucleoSpin RNA XS kit (Macherey-Nagel). The mRNAs of which the levels were $\geq$ 20-fold more in "After IP" than in "Before IP" were considered to be bound by the transfected miRNA.

miRNA overexpression and inhibition studies

miRNA mimics and inhibitors were commercially obtained from Qiagen. (1) *Mimics*: Syn-hsa-miR-29b-1-5p (cat. no. MSY0004514) and Syn-hsa-miR-503-5p (cat. no. MSY002874). (2) *Inhibitors*: anti-hsa-miR-612 (cat. no. MIN0003280), anti-hsa-miR-1208 (cat. no. MIN0005873), anti-hsa-miR-1231 (cat. no. MIN0005586) anti-hsa-miR-3185 (cat. no. MIN0015065). miRNA mimics and inhibitors were transfected either in 8-well chamber slides or in 12-well plates. The procedure is described in detail for the 8-well chamber slides. Alternate volumes or cell numbers for the transfection in 12-well plates are indicated in brackets. Shortly before the transfection, 10,000 (100,000) HSFs were seeded per well of an 8-well chamber slide in 250 (1,100) µL of serum-free DMEM. miRNA mimic [19 ng (75 ng)] or 190 ng (750 ng) inhibitor was diluted in 50 µL (100 µL) DMEM. This resulted in a final miRNA concentration of 5 nM (mimic) or 50 nM (inhibitor) after adding the complexes to the cells. HiPerfect Transfection Reagent [1.5 µL (6 µL); Qiagen] was added to the diluted miRNA and incubated for 10 min at room temperature to allow for the formation of transfection complexes. These complexes were added drop-wise onto the cells. The cells were incubated with the transfection complexes under regular growth conditions and analyzed after 48 h.

Indirect immunofluorescence

Indirect immunofluorescence was performed as previously described [26]. Briefly, HSFs were grown in 8-well chamber glass slides (Thermo Fisher Scientific) at densities of 10,000–75,000 cells/well, depending on the experiment. After fixation with 70% methanol/30% acetone and blocking with 10% v/v normal goat serum, the cells were incubated with one of the following primary antibodies: mouse monoclonal anti-actin (1:200; Sigma, cat. no. A4700), rabbit monoclonal anti-phosphorylated FAK antibody (Tyr397) (1:400; Abcam, cat. no. ab81298) and anti-p-Smad2 antibodies (Ser465/467) (1:500, Millipore, cat. no. AB3849). Secondary antibodies used were 1:100 diluted goat anti-rabbit or goat anti-mouse conjugated to Alexa Fluor 488 (Life Technologies, cat. no. A11008 and A11029) and goat anti-rabbit or goat anti-mouse conjugated to Cy3 (Jackson Immunoresearch Laboratories, cat. no. 111-165-003 and 111-166-003). Nuclear counterstaining was performed with 4′, 6-diamidino-2-phenylindole (DAPI).

To unify the shape of HSFs, which can influence focal adhesion formation, Y-shape micropattens with 1600-μm^2 area (Cytoo) were used. rF1M-WT and rF1M-RGA (25 µg/mL) were coated for 2 h at room

temperature, prior to seeding 60,000 HSFs in 4 mL medium in 35-mm petri dishes. After 24 h, HSFs were fixed with 70% methanol/30% acetone and stained as described above.

All images were recorded with the Zen 2012 software (Zeiss) using an Axio Imager M2 microscope (Zeiss) equipped with an ORCA-flash4.0 camera (Hamamatsu).

Quantification of p-Smad2 and focal adhesions

Quantification of p-Smad2 and of focal adhesions were performed using the ImageJ software [81]. To quantify p-Smad2, the corrected total cell fluorescence was determined. An outline was drawn around each cell, and area and mean fluorescence were measured. The background was determined in areas without cells. The corrected total cell fluorescence was calculated: CTCF = (mean fluorescence intensity of the cell – mean background intensity) × area of selected cell.

The quantification of focal adhesion was based on an established procedure which was adjusted in the following manner [82]. To decrease the background, the images were processed using "*Subtract Background*" with the sliding paraboloid option and 50 pixels rolling ball radius. To enhance the local contrast, the CLAHE plugin (Contrast Limited Adaptive Histogram Equalization) was used with these parameters: block size, 19; histogram bins, 256; and maximum slope, 6 [83]. To optimize the quality of images for particle quantification, "*Mathematical exponential*" (EXP), "*Brightness & Contrast*," and "*Threshold*" were sequentially applied. The "*min and max*" values of "*Brightness & Contrast*" and "*Threshold*" were derived from the average of the automatic values obtained from multiple images. The average "*min and max*" values were applied to all images. Finally, "*Analyze Particles*" produced the number, the average size and the total area of focal adhesions.

CRediT authorship contribution statement

Karina A. Zeyer: Conceptualization, Data curation, Investigation, Methodology, Validation, Visualization, Formal analysis, Writing - original draft, Writing - review & editing. **Rong-Mo Zhang:** Conceptualization, Data curation, Investigation, Methodology, Validation, Visualization, Formal analysis, Writing - original draft, Writing - review & editing. **Heena Kumra:** Data curation, Investigation, Methodology, Validation, Visualization, Formal analysis, Writing - review & editing. **Amani Hassan:** Data curation, Investigation, Methodology, Validation, Visualization, Formal analysis, Writing - review & editing. **Dieter P. Reinhardt:** Conceptualization, Formal analysis, Writing - review & editing, Funding acquisition, Project administration, Resources, Supervision.

Acknowledgments

This study was financially supported by the Natural Sciences and Engineering Research Council of Canada (RGPIN-2016-06278), the Heart and Stroke Foundation Canada (G-16-00014634), the Canadian Institutes of Health Research (MOP-137091), the Fonds de recherche du Québec—Nature et technologies, the Réseau de recherche en santé buccodentaire et osseuse, and fellowships from the German Studienstiftung des Deutschen Volkes, McGill University and the China Scholarship Council.

Conflict of Interest: The authors do not have a conflict of interest.

Appendix A. Supplementary data

Supplementary data to this article can be found online at https://doi.org/10.1016/j.jmb.2018.11.021.

Received 18 September 2018;
Received in revised form 30 October 2018;
Accepted 23 November 2018
Available online 28 November 2018

Keywords:
fibrillin;
integrin;
microRNA;
cell signaling;
extracellular matrix

†K.A.Z. and R.-M.Z. contributed equally to this work.

Abbreviations used:
BMP, bone morphogenetic protein; cbEGF, calcium-binding epidermal growth factor-like domain; DAVID, the database for annotation, visualization and integrated discovery; DIANA, DNA intelligent analysis; DMEM, Dulbecco's modified Eagle's medium; FAK, focal adhesion kinase; FDR, false determination rate; HEK293, human embryonic kidney 293; HSFs, human skin fibroblasts; KEGG, Kyoto encyclopedia of genes and genomes; LTBP, latent TGF-β binding protein; MAPK, mitogen-activated protein kinase; miRNA, micro-ribonucleic acid; p-Smad2, phosphorylated Sma and Mad related protein 2; TB, transforming growth factor-beta-binding protein-like domain; TBS, Tris-buffered saline; TGF-β, transforming growth factor-beta; UTR, untranslated regions.

References

[1] L.Y. Sakai, D.R. Keene, E. Engvall, Fibrillin, a new 350-kD glycoprotein, is a component of extracellular microfibrils, J. Cell Biol. 103 (1986) 2499–2509.

[2] B. Lee, M. Godfrey, E. Vitale, H. Hori, M.G. Mattei, M. Sarfarazi, et al., Linkage of Marfan syndrome and a phenotypically related disorder to two different fibrillin genes, Nature 352 (1991) 330–334.
[3] T. Nagase, M. Nakayama, D. Nakajima, R. Kikuno, O. Ohara, Prediction of the coding sequences of unidentified human genes. XXII. The complete sequences of 100 new cDNA clones from brain which code for large proteins in vitro, DNA Res. 8 (2001) 85–95.
[4] A. Piha-Gossack, W.S. Sossin, D.P. Reinhardt, The evolution of extracellular fibrillins and their functional domains, PLoS One 7 (2012), e33560.
[5] H. Zhang, W. Hu, F. Ramirez, Developmental expression of fibrillin genes suggests heterogeneity of extracellular microfibrils, J. Cell Biol. 129 (1995) 1165–1176.
[6] G.M. Corson, N.L. Charbonneau, D.R. Keene, L.Y. Sakai, Differential expression of fibrillin-3 adds to microfibril variety in human and avian, but not rodent, connective tissues, Genomics 83 (2004) 461–472.
[7] L. Sabatier, N. Miosge, D. Hubmacher, G. Lin, E.C. Davis, D. P. Reinhardt, Fibrillin-3 expression in human development, Matrix Biol. 30 (2011) 43–52.
[8] L. Pereira, M. D'Alessio, F. Ramirez, J.R. Lynch, B. Sykes, T. Pangilinan, et al., Genomic organization of the sequence coding for fibrillin, the defective gene product in Marfan syndrome, Hum. Mol. Genet. 2 (1993) 961–968.
[9] G.M. Corson, S.C. Chalberg, H.C. Dietz, N.L. Charbonneau, L.Y. Sakai, Fibrillin binds calcium and is coded by cDNAs that reveal a multidomain structure and alternatively spliced exons at the 5′ end, Genomics 17 (1993) 476–484.
[10] A.K. Downing, V. Knott, J.M. Werner, C.M. Cardy, I.D. Campbell, P.A. Handford, Solution structure of a pair of calcium-binding epidermal growth factor-like domains: implications for the Marfan syndrome and other genetic disorders, Cell 85 (1996) 597–605.
[11] X. Yuan, A.K. Downing, V. Knott, P.A. Handford, Solution structure of the transforming growth factor ß-binding protein-like module, a domain associated with matrix fibrils, EMBO J. 16 (1997) 6659–6666.
[12] R.O. Hynes, Integrins: bidirectional, allosteric signaling machines, Cell 110 (2002) 673–687.
[13] J.D. Humphries, A. Byron, M.J. Humphries, Integrin ligands at a glance, J. Cell Sci. 119 (2006) 3901–3903.
[14] T.D. Ross, B.G. Coon, S. Yun, N. Baeyens, K. Tanaka, M. Ouyang, et al., Integrins in mechanotransduction, Curr. Opin. Cell Biol. 25 (2013) 613–618.
[15] E.R. Horton, P. Astudillo, M.J. Humphries, J.D. Humphries, Mechanosensitivity of integrin adhesion complexes: role of the consensus adhesome, Exp. Cell Res. 343 (2016) 7–13.
[16] M. Pfaff, D.P. Reinhardt, L.Y. Sakai, R. Timpl, Cell adhesion and integrin binding to recombinant human fibrillin-1, FEBS Lett. 384 (1996) 247–250.
[17] H. Sakamoto, T. Broekelmann, D.A. Cheresh, F. Ramirez, J. Rosenbloom, R.P. Mecham, Cell-type specific recognition of RGD- and non-RGD-containing cell binding domains in fibrillin-1, J. Biol. Chem. 271 (1996) 4916–4922.
[18] D.V. Bax, S.E. Bernard, A. Lomas, A. Morgan, J. Humphries, A. Shuttleworth, et al., Cell adhesion to fibrillin-1 molecules and microfibrils is mediated by alpha5 beta1 and alphav beta3 integrins, J. Biol. Chem. 278 (2003) 34605–34616.
[19] J. Jovanovic, J. Takagi, L. Choulier, N.G. Abrescia, D.I. Stuart, P.A. van der Merwe, et al., αVß6 is a novel receptor for human fibrillin-1: comparative studies of molecular determinants underlying integrin-RGD affinity and specificity, J. Biol. Chem. 282 (2007) 6743–6751.
[20] D.V. Bax, Y. Mahalingam, S. Cain, K. Mellody, L. Freeman, K. Younger, et al., Cell adhesion to fibrillin-1: identification of an Arg-Gly-Asp-dependent synergy region and a heparin-binding site that regulates focal adhesion formation, J. Cell Sci. 120 (2007) 1383–1392.
[21] K. Tiedemann, B. Bätge, P.K. Müller, D.P. Reinhardt, Interactions of fibrillin-1 with heparin/heparan sulfate: implications for microfibrillar assembly, J. Biol. Chem. 276 (2001) 36035–36042.
[22] T.M. Ritty, T.J. Broekelmann, C.C. Werneck, R.P. Mecham, Fibrillin-1 and -2 contain heparin-binding sites important for matrix deposition and that support cell attachment, Biochem. J. 375 (2003) 425–432.
[23] S.A. Cain, C. Baldock, J. Gallagher, A. Morgan, D.V. Bax, A.S. Weiss, et al., Fibrillin-1 interactions with heparin: implications for microfibril and elastic fibre assembly, J. Biol. Chem. 280 (2005) 30526–30537.
[24] S.A. Cain, A.K. Baldwin, Y. Mahalingam, B. Raynal, T.A. Jowitt, C.A. Shuttleworth, et al., Heparan sulfate regulates fibrillin-1 N- and C-terminal interactions, J. Biol. Chem. 283 (2008) 27017–27027.
[25] D.A. Yadin, I.B. Robertson, J. McNaught-Davis, P. Evans, D. Stoddart, P.A. Handford, et al., Structure of the fibrillin-1 N-terminal domains suggests that heparan sulfate regulates the early stages of microfibril assembly, Structure 21 (2013) 1743–1756.
[26] D. Hubmacher, E. Bergeron, C. Fagotto-Kaufmann, L.Y. Sakai, D.P. Reinhardt, Early fibrillin-1 assembly monitored through a modifiable recombinant cell approach, Biomacromolecules 15 (2014) 1456–1468.
[27] J.E. Wagenseil, R.P. Mecham, New insights into elastic fiber assembly, Birth Defects Res. C. Embryo Today 81 (2007) 229–240.
[28] G. Raviola, The fine structure of the ciliary zonule and ciliary epithelium, Invest. Ophthalmol. 10 (1971) 851–869.
[29] W. Kriz, M. Elger, K. Lemley, T. Sakai, Structure of the glomerular mesangium: a biomechanical interpretation, Kidney Int. Suppl. 30 (1990) S2–S9.
[30] E.R. Neptune, P.A. Frischmeyer, D.E. Arking, L. Myers, T.E. Bunton, B. Gayraud, et al., Dysregulation of TGF-beta activation contributes to pathogenesis in Marfan syndrome, Nat. Genet. 33 (2003) 407–411.
[31] G. Sengle, N.L. Charbonneau, R.N. Ono, T. Sasaki, J. Alvarez, D.R. Keene, et al., Targeting of bone morphogenetic protein growth factor complexes to fibrillin, J. Biol. Chem. 283 (2008) 13874–13888.
[32] Z. Isogai, R.N. Ono, S. Ushiro, D.R. Keene, Y. Chen, R. Mazzieri, et al., Latent transforming growth factor beta-binding protein 1 interacts with fibrillin and is a microfibril-associated protein, J. Biol. Chem. 278 (2003) 2750–2757.
[33] H.C. Dietz, G.R. Cutting, R.E. Pyeritz, C.L. Maslen, L.Y. Sakai, G.M. Corson, et al., Marfan syndrome caused by a recurrent de novo missense mutation in the fibrillin gene, Nature 352 (1991) 337–339.
[34] B.L. Loeys, E.E. Gerber, D. Riegert-Johnson, S. Iqbal, P. Whiteman, V. McConnell, et al., Mutations in fibrillin-1 cause congenital scleroderma: stiff skin syndrome, Sci. Transl. Med. 2 (2010) 23ra20.
[35] C. Le Goff, C. Mahaut, L.W. Wang, S. Allali, A. Abhyankar, S. Jensen, et al., Mutations in the TGFß binding-protein-like domain 5 of FBN1 are responsible for acromicric and

geleophysic dysplasias, Am. J. Hum. Genet. 89 (2011) 7–14.
[36] L. Faivre, R.J. Gorlin, M.K. Wirtz, M. Godfrey, N. Dagoneau, J.R. Samples, et al., In frame fibrillin-1 gene deletion in autosomal dominant Weill–Marchesani syndrome, J. Med. Genet. 40 (2003) 34–36.
[37] J.P. Habashi, D.P. Judge, T.M. Holm, R.D. Cohn, B.L. Loeys, T.K. Cooper, et al., Losartan, an AT1 antagonist, prevents aortic aneurysm in a mouse model of Marfan syndrome, Science 312 (2006) 117–121.
[38] D.P. Bartel, MicroRNAs: genomics, biogenesis, mechanism, and function, Cell 116 (2004) 281–297.
[39] W. Filipowicz, S.N. Bhattacharyya, N. Sonenberg, Mechanisms of post-transcriptional regulation by microRNAs: are the answers in sight? Nat. Rev. Genet. 9 (2008) 102–114.
[40] E. Bernstein, S.Y. Kim, M.A. Carmell, E.P. Murchison, H. Alcorn, M.Z. Li, et al., Dicer is essential for mouse development, Nat. Genet. 35 (2003) 215–217.
[41] M. Ha, V.N. Kim, Regulation of microRNA biogenesis, Nat. Rev. Mol. Cell Biol. 15 (2014) 509–524.
[42] Z.J. Rutnam, T.N. Wight, B.B. Yang, miRNAs regulate expression and function of extracellular matrix molecules, Matrix Biol. 32 (2013) 74–85.
[43] M. Climent, M. Quintavalle, M. Miragoli, J. Chen, G. Condorelli, L. Elia, TGFbeta triggers miR-143/145 transfer from smooth muscle cells to endothelial cells, thereby modulating vessel stabilization, Circ. Res. 116 (2015) 1753–1764.
[44] M. Xin, E.M. Small, L.B. Sutherland, X. Qi, J. McAnally, C.F. Plato, et al., MicroRNAs miR-143 and miR-145 modulate cytoskeletal dynamics and responsiveness of smooth muscle cells to injury, Genes Dev. 23 (2009) 2166–2178.
[45] D.R. Merk, J.T. Chin, B.A. Dake, L. Maegdefessel, M.O. Miller, N. Kimura, et al., miR-29b participates in early aneurysm development in Marfan syndrome, Circ. Res. 110 (2012) 312–324.
[46] L. Maegdefessel, J. Azuma, R. Toh, D.R. Merk, A. Deng, J.T. Chin, et al., Inhibition of microRNA-29b reduces murine abdominal aortic aneurysm development, J. Clin. Invest. 122 (2012) 497–506.
[47] D. Hubmacher, E. El-Hallous, V. Nelea, M.T. Kaartinen, E.R. Lee, D.P. Reinhardt, Biogenesis of extracellular microfibrils: multimerization of the fibrillin-1 C-terminus into bead-like structures enables self-assembly, Proc. Natl. Acad. Sci. U. S. A. 105 (2008) 6548–6553.
[48] I.S. Vlachos, N. Kostoulas, T. Vergoulis, G. Georgakilas, M. Reczko, M. Maragkakis, et al., DIANA miRPath v.2.0: investigating the combinatorial effect of microRNAs in pathways, Nucleic Acids Res. 40 (2012) W498–W504.
[49] D. Betel, A. Koppal, P. Agius, C. Sander, C. Leslie, Comprehensive modeling of microRNA targets predicts functional non-conserved and non-canonical sites, Genome Biol. 11 (2010) R90.
[50] X.A. Cambronne, R. Shen, P.L. Auer, R.H. Goodman, Capturing microRNA targets using an RNA-induced silencing complex (RISC)-trap approach, Proc. Natl. Acad. Sci. U. S. A. 109 (2012) 20473–20478.
[51] P. Hartmann, Z. Zhou, L. Natarelli, Y. Wei, M. Nazari-Jahantigh, M. Zhu, et al., Endothelial Dicer promotes atherosclerosis and vascular inflammation by miRNA-103-mediated suppression of KLF4, Nat. Commun. 7 (2016) 10521.
[52] R. Wilson, C. Espinosa-Diez, N. Kanner, N. Chatterjee, R. Ruhl, C. Hipfinger, et al., MicroRNA regulation of endothelial TREX1 reprograms the tumour microenvironment, Nat. Commun. 7 (2016) 13597.
[53] J.E. Braun, E. Huntzinger, E. Izaurralde, The role of GW182 proteins in miRNA-mediated gene silencing, Adv. Exp. Med. Biol. 768 (2013) 147–163.
[54] J. Takagi, K. Strokovich, T.A. Springer, T. Walz, Structure of integrin α5β1 in complex with fibronectin, EMBO J. 22 (2003) 4607–4615.
[55] S. Aota, M. Nomizu, K.M. Yamada, The short amino acid sequence Pro-His-Ser-Arg-Asn in human fibronectin enhances cell-adhesive function, J. Biol. Chem. 269 (1994) 24756–24761.
[56] S. Johansson, G. Svineng, K. Wennerberg, A. Armulik, L. Lohikangas, Fibronectin–integrin interactions, Front. Biosci. 2 (1997) d126–d146.
[57] C. Steentoft, S.Y. Vakhrushev, H.J. Joshi, Y. Kong, M.B. Vester-Christensen, K.T. Schjoldager, et al., Precision mapping of the human *O*-GalNAc glycoproteome through SimpleCell technology, EMBO J. 32 (2013) 1478–1488.
[58] S.S. Chaudhry, S.A. Cain, A. Morgan, S.L. Dallas, C.A. Shuttleworth, C.M. Kielty, Fibrillin-1 regulates the bioavailability of TGF-beta1, J. Cell Biol. 176 (2007) 355–367.
[59] E.E. Gerber, E.M. Gallo, S.C. Fontana, E.C. Davis, F.M. Wigley, D.L. Huso, et al., Integrin-modulating therapy prevents fibrosis and autoimmunity in mouse models of scleroderma, Nature 503 (2013) 126–130.
[60] E. van Rooij, L.B. Sutherland, J.E. Thatcher, J.M. Dimaio, R.H. Naseem, W.S. Marshall, et al., Dysregulation of microRNAs after myocardial infarction reveals a role of miR-29 in cardiac fibrosis, Proc. Natl. Acad. Sci. U. S. A. 105 (2008) 13027–13032.
[61] B. Maurer, J. Stanczyk, A. Jungel, A. Akhmetshina, M. Trenkmann, M. Brock, et al., MicroRNA-29, a key regulator of collagen expression in systemic sclerosis, Arthritis Rheum. 62 (2010) 1733–1743.
[62] A.J. Kriegel, Y. Liu, Y. Fang, X. Ding, M. Liang, The miR-29 family: genomics, cell biology, and relevance to renal and cardiovascular injury, Physiol. Genomics 44 (2012) 237–244.
[63] J.S. Yang, M.D. Phillips, D. Betel, P. Mu, A. Ventura, A.C. Siepel, et al., Widespread regulatory activity of vertebrate microRNA* species, RNA 17 (2011) 312–326.
[64] S. Bell, E.M. Terentjev, Focal adhesion kinase: the reversible molecular mechanosensor, Biophys. J. 112 (2017) 2439–2450.
[65] P.J. Wipff, B. Hinz, Integrins and the activation of latent transforming growth factor beta1—an intimate relationship, Eur. J. Cell Biol. 87 (2008) 601–615.
[66] J.L. Duband, M. Gimona, M. Scatena, S. Sartore, J.V. Small, Calponin and Sm22 as differentiation markers of smooth-muscle—spatiotemporal distribution during avian embryonic development, Differentiation 55 (1993) 1–11.
[67] B. Hinz, V. Dugina, C. Ballestrem, B. Wehrle-Haller, C. Chaponnier, Alpha-smooth muscle actin is crucial for focal adhesion maturation in myofibroblasts, Mol. Biol. Cell 14 (2003) 2508–2519.
[68] B. Geiger, A. Bershadsky, R. Pankov, K.M. Yamada, Transmembrane crosstalk between the extracellular matrix–cytoskeleton crosstalk, Nat. Rev. Mol. Cell Biol. 2 (2001) 793–805.
[69] G. Lin, K. Tiedemann, T. Vollbrandt, H. Peters, B. Bätge, J. Brinckmann, et al., Homo- and heterotypic fibrillin-1 and -2 interactions constitute the basis for the assembly of microfibrils, J. Biol. Chem. 277 (2002) 50795–50804.
[70] R. Kirschner, D. Hubmacher, G. Iyengar, J. Kaur, C. Fagotto-Kaufmann, D. Brömme, et al., Classical and neonatal Marfan syndrome mutations in fibrillin-1 cause differential protease

susceptibilities and protein function, J. Biol. Chem. 286 (2011) 32810–32823.
[71] K.T. Mellody, L.J. Freeman, C. Baldock, T.A. Jowitt, V. Siegler, B.D. Raynal, et al., Marfan syndrome-causing mutations in fibrillin-1 result in gross morphological alterations and highlight the structural importance of the second hybrid domain, J. Biol. Chem. 281 (2006) 31854–31862.
[72] C.M. Cardy, P.A. Handford, Metal ion dependency of microfibrils supports a rod-like conformation for fibrillin-1 calcium-binding epidermal growth factor-like domains, J. Mol. Biol. 276 (1998) 855–860.
[73] D.P. Reinhardt, D.R. Keene, G.M. Corson, E. Pöschl, H.P. Bächinger, J.E. Gambee, et al., Fibrillin 1: organization in microfibrils and structural properties, J. Mol. Biol. 258 (1996) 104–116.
[74] J. Kaur, D.P. Reinhardt, Immobilized metal affinity chromatography co-purifies TGF-beta1 with histidine-tagged recombinant extracellular proteins, PLoS One 7 (2012), e48629.
[75] T.L. Morgan, D.J. Yang, D.G. Fry, P.J. Hurlin, S.K. Kohler, V.M. Maher, et al., Characteristics of an infinite life span diploid human fibroblast cell strain and a near-diploid strain arising from a clone of cells expressing a transfected v-myc oncogene, Exp. Cell Res. 197 (1991) 125–136.
[76] J. Wegener, C.R. Keese, I. Giaever, Electric cell-substrate impedance sensing (ECIS) as a noninvasive means to monitor the kinetics of cell spreading to artificial surfaces, Exp. Cell Res. 259 (2000) 158–166.
[77] Y. Benjamini, Y. Hochberg, Controlling the false discovery rate—a practical and powerful approach to multiple testing, J. R. Stat. Soc. Ser. B Stat Methodol. 57 (1995) 289–300.
[78] R. Edgar, M. Domrachev, A.E. Lash, Gene expression omnibus: NCBI gene expression and hybridization array data repository, Nucleic Acids Res. 30 (2002) 207–210.
[79] T. Barrett, S.E. Wilhite, P. Ledoux, C. Evangelista, I.F. Kim, M. Tomashevsky, et al., NCBI GEO: archive for functional genomics data sets–update, Nucleic Acids Res. 41 (2013) D991–D995.
[80] D.W. Huang, B.T. Sherman, R.A. Lempicki, Systematic and integrative analysis of large gene lists using DAVID bioinformatics resources, Nat. Protoc. 4 (2009) 44–57.
[81] C.A. Schneider, W.S. Rasband, K.W. Eliceiri, NIH Image to ImageJ: 25 years of image analysis, Nat. Methods 9 (2012) 671–675.
[82] U. Horzum, B. Ozdil, D. Pesen-Okvur, Step-by-step quantitative analysis of focal adhesions, MethodsX 1 (2014) 56–59.
[83] K. Zuiderveld, Contrast limited adaptive histogram equalization, in: P.S. Heckbert (Ed.), Graphics Gems IV, Academic Press Professional 1994, pp. 474–485.
[84] D.W. Huang, B.T. Sherman, R.A. Lempicki, Bioinformatics enrichment tools: paths toward the comprehensive functional analysis of large gene lists, Nucleic Acids Res. 37 (2009) 1–13.